AN INVESTIGATION OF THERMAL COMFORT AND ASYMMETRIC TRANSPORT PROPERTIES IN ELECTROSPUN NANOFIBER MATERIALS

A Thesis

Presented to the Faculty of the Graduate School

of Cornell University

In Partial Fulfillment of the Requirements for the Degree of

Master of Science

by

Robert Duryee Flint

May 2015

ABSTRACT

The human clothing environment exists in a constant state of fluctuation, as heat and moisture is continuously exchanged between the body and its surroundings. Thermal insulation and breathability are considered the two most important factors controlling the exchange of heat and moisture while gas permeability and water vapor diffusion are the most important transport properties used to correlate thermal comfort.

Laminated fabrics, such as Gore-Tex®, have long been favored by the outdoor industry at large. The pores in Gore-Tex® ePTFE membranes are small enough to block drops of liquid water yet large enough to allow the much smaller water vapor molecules to passively diffuse through. Careful examinations of existing transport property models suggest membranes with smaller fiber diameters, fiber alignment and specially engineered pore structures may offer improved membrane performance.

This thesis explores the effect of fiber diameter, fiber alignment, and multilayered constructions on key transport properties. In-plane fiber alignment was found to have no significant effect on air permeability or water vapor diffusion. Multilayered constructions with increasing pore sizes were found to exhibit directional preference or asymmetric transport for both air permeability and water vapor diffusion. Three theories are discussed and future work is proposed.

BIOGRAPHICAL SKETCH

Sandy grew up in the hills of Western Massachusetts. He attended Colorado College and received a Bachelor of Arts degree in physics and mathematics in 2008. Inspired by the natural beauty of the western landscape, he spent three years working in Colorado, Utah, Idaho, Washington, Montana and Wyoming as an outdoor educator. During this time he found a home in the mountains and on the great rivers of the American West. Exposed to an array of sport specific gear through these hands on experiences, he began the Fiber Science & Apparel Design program at Cornell University to better understand the construction materials and manufacturing techniques required to make quality outdoor apparel.

To my parents and siblings for teaching me how to grow fresh bone marrow; you can accomplish anything if you waste enough time doing it.

ACKNOWLEDGMENTS

First, I would like to thank my advisor, Professor Huiju Park, for sharing his expertise, time, and sound advice throughout the course of my time here at Cornell. I would also like to thank Professor Jintu Fan, for inviting me to join his weekly research meetings and supporting my research. It was truly a pleasure to work with such a smart, thoughtful and funny group of fellow graduate students. I cherish your comradely. The generous and insightful contributions of Dahau "Rock" Shou were pivotal in reaching this investigation's full potential. Thank you. Last, but certainly not least, completing my thesis would have been impossible without the hugs, smiles, late night discussions and constant support of Hilary Byerly. I love you.

TABLE OF CONTENTS

LIST OF FIGURES

LIST OF TABLES

1 Introduction

The human clothing environment exists in a constant state of fluctuation, as heat and moisture is continuously exchanged between the body and its surroundings. This exchange takes place on the surface of the skin through processes of convection, radiation, conduction and evaporation (Holmér, 2005). Though the human body can naturally balance thermoregulation within a narrow range of external conditions using physiological mechanisms (goose bumps to slow airflow over the skin, shivering resulting in exothermic reactions in muscle cells, constriction of blood vessels to restrict blood flow to superficial capillaries), a key functionality of clothing is to broaden the comfort range. Material transport properties are thus an important consideration when designing clothing and a solid understanding of textile transport properties and how, as garments, they shape the interaction between the body and environment is the foundation on which performance clothing is constructed.

Thermal insulation and breathability are considered the two most important factors controlling the exchange of heat and moisture between the body and its surrounding environment (Williams, 2009). When the human body experiences minimal activity, dry heat exchanges (conduction, convection, radiation) are the dominant heat loss mechanisms governing thermal regulation. As physical activity increases, sensible perspiration forms on the skin and evaporative cooling takes over. Clothing designers for active wear applications must therefore be considerate of a textile's breathability properties. If water vapor from evaporative cooling is unable to quickly diffuse through clothing, the increase in microclimate relative humidity can cause increased thermal

conductivity of the insulating air within the clothing system, making the clothing uncomfortable.

In cold environments, achieving thermal comfort is particularly challenging as inherent trade offs exist between protection and breathability. Laminated fabrics, such as Gore-Tex®, have long been favored by the outdoor industry at large. Gore-Tex® is constructed by bonding a thin microporous membrane onto traditionally woven face fabrics. The pores in the membrane are small enough to block drops of liquid water yet large enough to allow the much smaller water vapor molecules to passively diffuse through. The expiration of Gore's patent unleashed a flood of newcomers who have developed their own waterproof-breathable fabrics (e.g., Sympatex®, Polartec's NeoShell®, Columbia's OmniDry®, and Marmot's Membrain™), each eager to get in on the billion-dollar market (Kessler, 2012). Constantly looking for a performance edge, one possible solution to improve the breathability of these fabrics may be discovered in using a new membrane.

Careful examinations of existing transport property models suggest membranes with smaller fiber diameters, fiber alignment and specially engineered pore structures may offer improved performance (Shou, Fan, & Ding, 2013). Electrospinning is a novel process capable of spinning polymer solutions into fibers with extremely small diameters on the nanoscale (Chowdhury & Stylios, 2010). Together, these fiber form super thin nonwoven membrane-like nanowebs with high porosity and incredibly small pore size (Gibson, Schreuder-Gibson, & Rivin, 2001a). The use of electrospun membranes in protective clothing and athletic apparel has previously been investigated (Ahn, H.W., Park, C.H., & Chung, S.E., 2011; Gibson et al., 2001a; Seungsin Lee & Obendorf, 2007;

Yoon & Lee, 2011). The researchers identified a "window of opportunity" for new materials with both high barrier strength and good comfort performance. Electrospun mats demonstrate encouraging air and moisture permeability, offering minimal impedance to moisture vapor diffusion that compare favorably with transport properties of conventional waterproof-breathable fabrics.

Randomly aligned fibers generally have higher air permeability than ordered fibers because they are made up of a mixture of large and small pore sizes (large pores dominate gas permeability). Improved electrospinning setups have given researchers more control of fiber orientation (Carnell et al., 2008), however the resulting effect of in-plane fiber orientation on transport properties has not been thoroughly studied. It is thus hypothesized aligned nanofibers may offer lower air permeability, a desirable property for many applications, than random nanofibers. To help further the development of electrospun membranes, more knowledge of the effect of fiber alignment on transport properties is of great interest.

Specialized models can be employed to verify these improved transport properties. Modeling transport properties through fabric structures helps researchers better understand gas flow in multi-layered constructions and provide brands a platform for quantitative analysis. The basic principles of gas flow though unidirectional fibers have widely been understood and studied for over 50 years. When these same principles are applied to fibers on the nanoscale however, classic theories prove to be inadequate (Shou, Ye, & Fan, 2014). Researchers have identified these shortcomings and have developed models to account for the influences of random fiber distribution and slip flow.

Experimental verification of these models with different materials is important to strengthen their validity.

Finally, research and development energy has recently been focused on directional transport properties induced by engineered pore shapes. From applications in particle filtration to the breathable protective clothing, directional preference of through-plane flow holds great potential in a wide range of scientific and industrial applications. Similar to plant transpiration, negative capillary pressure generated by pore geometry can help drive fluids through textile materials. While substantial research has been focused on liquid transport, transport of air and water vapor is generally assumed to be directionally uniform.

1.1 Objectives

Based on the identified research gaps, the aim of this study can be broken into three unique objectives. First, the impact fiber diameter and fiber alignment have on transport properties affecting breathability (air permeability and water vapor permeability) will be investigated using nylon 6 electrospun membranes. Next, previously developed models that describe gas flow and vapor diffusion in nanofiber materials will be used to both confirm the experimental transport data and strengthen the validity of models themselves. Lastly, this research will explore the directional capacity of airflow and water vapor transport in multilayered nanofiber/nanofiber and nanofiber/microfiber nonwoven materials.

2 Background and Justification

2.1 Environmental Challenges and Thermal Comfort

Climatic conditions on earth are variable. Extreme weather data report historical temperature highs of 56.7˚C (134˚F) and lows of -89.2˚C (-128.6˚F) ("Weather Records," 2015). Variation of this magnitude is far more than the human body can tolerate alone. To compensate for extreme conditions, clothing systems have been developed to protect the body from external conditions, control sensible heat loss (or gain), and maintain thermal regulation. The resulting human clothing environment exists in a dynamic state of fluctuation, as heat and moisture are continuously exchanged between the body and the surrounding environment in an effort to maintain an average core body temperature of 37˚C (Mackowiak, 2000).

Thermal comfort is a condition or feeling achieved when complex interactions between highly subjective human sensations, clothing systems and the surrounding environment are in equilibrium. The International Organization for Standardization defines thermal comfort as a "condition of mind which expressed satisfaction with the thermal environment" (ISO 7730, 1994). Thermal comfort cannot be reached when the body is too cold or too warm or when perspiration produced by the body cannot be freely evaporated and transported to the surrounding environment. In simple subjective measurements, thermal comfort is obtained when minimal physiological effort is required to maintain a core body temperature of 37˚C, which typically dictates a mean skin temperature of 33-35˚C, and the average wetted skin area is no more than 30% (Williams, 2009).

When layered clothing systems are draped on the human body, they create a volume of enclosed air that acts as a barrier for both heat and moisture transport between the body and the environment (Havenith, 1999). Together, the body, clothing and environment form a dynamic microclimate, with a constant exchange of energy (heat) and mass (liquids and gases) (Pan, 2008). Creating and maintaining a stable microclimate is critical to achieving thermal comfort and a key aspect of performance clothing (Das, Das, Kothari, Fanguiero, & De Araújo, 2008; Onofrei, Rocha, & Catarino, 2011).

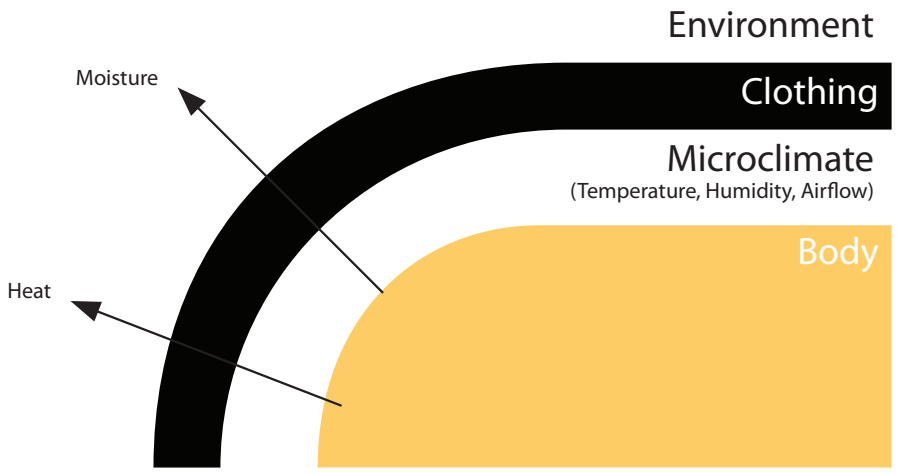

Figure 2.1 Enclosed air between clothing and the human body creates a dynamic microclimate.

Two persistent gradients, temperature and moisture, exist between the body, microclimate and the surrounding environment and together, they largely dictate thermal comfort. The amount of heat and moisture exchanged between the two can be quantified by testing both thermal insulation and breathability (Ghaddar, Ghali, & Williams, 2009). While physical activity and environmental conditions must also be considered, thermal insulation and breathability are the

two most important material properties regularly used to correlate textile materials with thermal comfort (Obendorf, 2010).

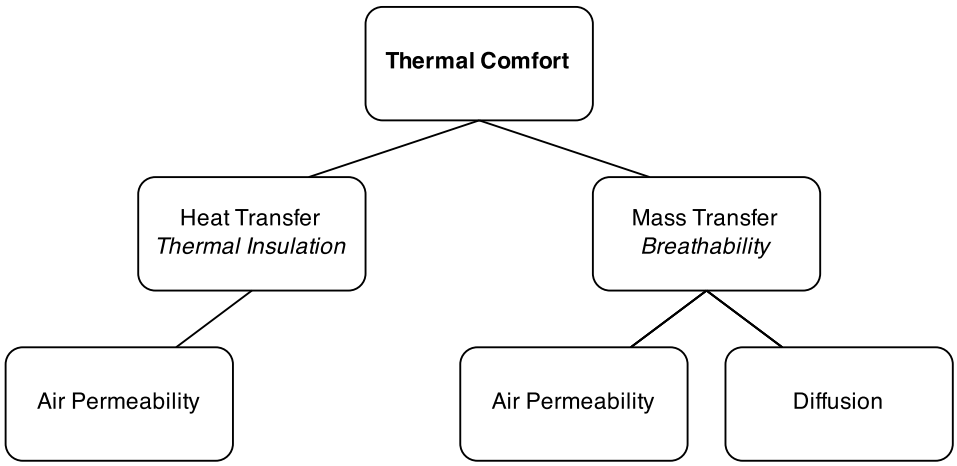

Figure 2.2. Air permeability and water vapor diffusion transport properties are used to correlate thermal comfort.

Thermal insulation is a measurement that is used to quantify the ability of a material to reduce heat transfer between two objects. It is largely influenced by the materials ability to entrap still air, since still air has a thermal resistance eight times greater than most fibrous material (G. Song, 2009). Air is the primary insulator for many common clothing insulation materials, such as down, wool and fleece. Thermal insulation of bulk materials is a combination of their thermal conductivity, density and specific heat capacity.

Breathability, or how readily a material permits gas and liquid transport, also plays an important role in thermal comfort. If water vapor from evaporative cooling is unable to quickly diffuse through clothing, it causes an increase in microclimate humidity that increases the thermal conductivity of the fibers and insulating air within the clothing system, making the clothing uncomfortable.

Physiological studies have found surprisingly strong discomfort sensations associated with small amounts of water added to near the skin clothing (Scheurell, Spivak, & Hollies, 1985). Performance metrics are also negatively affected when water vapor becomes trapped in the microclimate; the amount of time a person can withstand strenuous work has been noted to decreases linearly with clothing water vapor permeability (Haghi, 2011). The same body of work also cited a 60% decrease in maximum subject performance when wearing an impermeable vapor barrier.

For clothing applications, breathability is quantified using two mass transport properties, air permeability and water vapor diffusion. Both transport properties are a function of the material's solid fiber volume (or it's inverse, porosity) and to a lesser degree, the fiber arrangement (Ghali, Ghaddar, & Jones, 2006). Additionally, for materials with extremely small fibers, theoretical models suggest gas permeability is also a function of fiber radius (Shou et al., 2014).

2.2 Heat Balance

Clothing provides protection by maintaining heat balance between the body and the environment (Havenith, 1999). Heat balance is a function of heat gain (metabolic heat generation, external mechanical work performed by the body, radiant heat gained from the environment) and heat loss exchanges that takes place on the surface of the skin (radiation, convection, conduction and evaporation (Holmér, 2005)). For temperature regulation to be stable, the amount of heat produced by the body and gained from the environment (if any) must be equal to the amount of natural heat loss. The rate of heat storage within the body can thus be summarized using the basic heat balance equation:

$$S = M - W - R - C - E — K - RES \qquad [\frac{W}{m^2}]$$

where:

S = rate of heat storage

M = rate of metabolic heat production

W = rate of mechanical work accomplished

R = radiant heat exchange

C = convective heat exchange

E = evaporative heat loss

K = conductive heat loss

RES = respiratory heat loss

If the rate of metabolic heat production is greater than the sum of all heat losses, heat storage S will be positive, which will cause the body temperature to rise. Similarly, if heat storage S is negative, the body is loosing more heat than is being produced and the body will cool (Havenith, 1999).

2.2.1 Heat Production

Heat production comes from three main sources: metabolic heat production, radiant heat absorption, and mechanical work (or physical activity). The majority of heat produced is a result of metabolic heat production, which is fueled by calories supplied by metabolized food. Greater activity causes the body to burn more calories, resulting in an increase in metabolic heat generation.

Table 2.1 Average metabolic rate (in Watts meter squared) for various activities. Greater metabolic activity leads to increased production of heat and moisture.

Activity	Average metabolic rate (Wm^2)
Resting: sitting at ease	65
Light manual work; casual walking (speed up to 3.5 km/h); spectators outdoors; winter fishing; scooter driving	100
Moderate work with hand and arm; arm and leg; walking at a speed of 3.5 km/h to 5.5 km/hr; hiking; alpine skiing	165
Intense arm and trunk work; carrying heavy material; walking at a speed of 5.5 km/h to 7 km/h; intermittent activity (ball games); slow walking in deep snow	230
Very intense activity at fast pace; climbing; running or walking at a speed greater than 7 km/h; alpine skiing (well trained)	290
Sustained heavy work; long distance events in cross country skiing	400

Adapted from *Cold weather clothing and comfort* in *Improving Comfort in Clothing* p. 414, by I. Holmér and edited by G. Song, 2011. Woodhead Publishing. (Guowen Song, 2011)1)

2.2.2 Heat Loss

As described in the heat balance equation, heat loss occurs through three avenues: dry heat loss or heat transport (conduction, convection, radiation), wet heat loss or mass transport (evaporation) or a combination of the two (respiratory heat loss). Insulated clothing is regularly worn to offset dry heat loss while breathable materials are important moisture management considerations to enable evaporative cooling. Though respiratory heat loss is significant in low ambient temperatures and where it must be considered, it occurs continuously as a function of breathing, and will only have limited consideration in this body of work.

Human bodies maintain thermal balance during most moderate activities and climatic conditions simply with dry heat transfer. When wind penetrates the

outer layer of a clothing system, it causes an increase in ventilation to occur in the microclimate (Holmer, 2011) that consequentially causes an increase in convective heat loss that may jeopardize thermal comfort. To minimize microclimate ventilation clothing should be windproof, as measured by the air permeability.

Radiant heat loss (R) occurs when there is a large radiant heat gradient between the radiant temperature of the immediate environment (t_r) and the mean weighted skin temperature ($\bar{t}_{sk}$). It is largely due to infrared emission and is more noticeable in cold weather, especially after sunset when there is little radiant heat absorption from the sun to offset the heat loss.

Convective heat loss (C) occurs between the skin and the ambient air surrounding a person. In outdoor clothing, convective heat loss primarily happens when the warm air next to the skin and trapped in the clothing system is displaced by cooler air from the surrounding environment. It can also occur more passively, via the chimney effect, a phenomenon that is the result of warm air rising through the clothing system and out the collar, thereby drawing cool air in through lower openings such as the waist opening and pant cuffs. Convective heat loss is a function of air velocity and the difference between the ambient air temperature (t_a) and the average skin temperature ($\bar{t}_{sk}$). As air velocity increases (ie wind, movement) convective heat loss also increases. Similarly, when the ambient temperature is greater than 35˚C body heat will increase but when ambient temperature is less than 35˚C, heat will be lost from the body to the environment by convection. The relationship of convective heat loss can be calculated using the following equation:

$$C = h_c V_a (t_a - \bar{t}_{sk}) \quad \left[\frac{W}{m^2}\right]$$

where h_c is the convective heat transfer coefficient, and V_a is the relative velocity of air.

Conductive heat loss (K), the transfer of heat between two objects in contact with one another, is an important consideration for outdoor clothing (as the fibers of the clothing are in contact with the skin), especially in cold environments where the temperature gradient between the environment and the skin surface is greatest. Conductive heat loss is greatest when the fiber volume fraction is relatively high (as the tiny pores are blocked, thus reducing the effect of convective heat loss).

As muscle activity increases, dry heat transfer becomes inadequate and additional cooling is required to dissipate heat from the body, ***evaporative cooling*** becomes the primary method to shed excess heat. Evaporative cooling is an important, dominant and effective thermoregulatory mechanism in warm weather and cold weather. In both environments however, sweat production and evaporative cooling can quickly become counterproductive and a challenge to manage.

Human bodies produce sweat in the form of sensible and insensible perspiration. We are often unaware of insensible perspiration however, as it occurs continuously and evaporates from the skin before it is perceived as moisture. Sensible perspiration occurs as a response to rising body temperatures. After sensible perspiration forms on the skin, it evaporates into water vapor. This transition of liquid to gas causes latent heat (the energy required to cause a phase change) to be absorbed, resulting in a strong cooling effect.

Be it a result of environmental conditions or intense activity, once the core body temperature reaches 37˚C, sensible perspiration is almost immediately produced on the skin (Pan, 2008). Depending on the activity, 2,280 – 45,600 g of moisture can be produced over the course of 24 hours. One gram of water will absorb 2260 joules of heat energy from the body in the process of evaporation. In cold environments when evaporative cooling post activity can lead to chilling, it is of utmost importance that water vapor quickly evaporated and diffused through cold weather clothing (Rengasamy, 2011).

Table 2.2 Metabolic moisture production (perspiration) for various activity levels. Moisture must be able to quickly diffuse through the clothing to avoid sensations of discomfort.

Activity	Metabolic Moisture Production g/24hrs
Resting	2280
Sitting	3800
Walking, normal	7600
Walking, quickly	11500
Walking, with light pack	15200
Walking, with heavy pack	19000
Walking, in mountains with heavy backpack	22800-30400
Mean maximum work rate	38000-45600

Table adapted from *Heat and Moisture Transfer in Textiles with Particular Reference to Clothing Comfort*, by A.K. Haghi in Heat and Mass Transfer, Second Edition, p. 86 (Haghi, 2011).

Condensation: During periods of heightened activity in cold climates, both body temperature and the rate of perspiration can increase to the point that the vapor transmission rate of the garment can no longer remove all the water vapor being generated. When this occurs, the microclimate inside the clothing system becomes relatively hot and humid compared to the outside environment.

Steep temperature gradients between the skin and the environment often lead to condensation, as the dew point is reached in the outer layers of the clothing system(Holmer, 2011).

Moisture buildup highlights the importance that cold weather clothing has good breathability, as the presence of condensation has several negative impacts on thermal comfort (Rossi, B, 2009). First, water helps collapse insulation materials, increasing the solid fraction while decreasing the thermal insulation. Second, as water droplets eventually merge into one connected film, evaporation is slowed and the area of wetness causes a sense of discomfort (Rengasamy, 2011). Finally, wetting fibers increases thermal conductivity of insulating material, as the thermal conductivity of water is approximately 24 times that of the conductivity of the air. Depending on the material, the difference can result in clothing nearly 30 times more conductive (see Table 2.3) (Pan, 2008). Higher thermal conductivity of wet clothing increases the chances of post exercise chilling (Ghali et al., 2006). When designing protective clothing, materials with higher water vapor transport rates are therefore desired, to reduce unwanted moisture buildup.

Table 2.3 Thermal conductivity of common textile materials, water, and silver. Note the thermal conductivity of water is much greater than the natural and synthetic textile materials.

Material	Thermal Conductivity ($Wm^{-1}K^{-1}$)
Cotton	0.10
Nylon	0.25
Polyester	0.14
Polypropylene	0.12
Still air	0.026
Water	0.6
Silver	418

Table adapted from *Physical Properties of Textile Fibers* (Morton & Hearle, 2008)

2.3 Waterproof Breathable Materials

Beginning in the 1960s-70s, development of waterproof materials trended towards lighter and more packable options. A solution was adopted laminating breathable membranes onto woven face fabrics in a multilayer construction. To maintain a comfortable balance for the wearer, waterproof breathable fabrics have been used extensively in outdoor apparel applications to provide protection from external moister such as rain (liquid water molecules ≈ 100μm diameter) while effectively transporting water vapor from evaporation (water vapor molecules ≈ 0.0004μm diameter) from inside the clothing to the outside environment (Ahn, H.W. et al., 2011; Yoon & Lee, 2011). There are two categories of laminated membrane fabrics in use today: microporous materials and nonporous hydrophilic materials. Laminated microporous materials and coated fabrics transport water vapor through small holes (that are much smaller than the size of the smallest raindrop (100μm)). Water vapor molecules pass through microporous membranes via the process of diffusion. This transport process is considered "passive transport", as the membrane plays no active role. Nonporous hydrophilic materials on the other hand rely on co-polymer membranes that harness the chemical process of adsorption to transport water vapor through the "soft" polymer chains segments (polyether, poly(ethylene) oxide) while the "hard" segments (ester, amide, or most commonly urethane residues) repel water droplets (R. Lomax, 2009; Yoon & Lee, 2011).

There are many different methods used for laminated fabrics and certain trade offs in the performance and cost. Table 2.4 summarizes commonly used

construction materials for waterproof applications that are currently available on the market.

Table 2.4 Popular waterproof garment construction materials

Material	Construction	Pros/Cons
Rubber/Vinyl	Solid plastic	**Pros**: Absolutely waterproof; good durability; inexpensive; good for sedentary activities **Cons**: Zero breathability; inappropriate for active use
Coated Nylon	Nylon fabric sprayed w/ waterproof coating	**Pros**: Lighter than rubber; pack down small **Cons**: "Waterproofness" and "breathability" decreases in long exposure to rain; not the best performance in either category
2-Layer	Face fabric laminated w/ waterproof membrane	**Pros**: Good for lifestyle clothing; lightweight; relatively inexpensive **Cons**: Poor abrasion resistance on inside; membrane needs to be protected by separate loose hanging fabric, which increases weight; largely replaced by 2.5 layer
2.5-Layer	Similar to 2-layer with printed "3D" pattern on inside to protect membrane	**Pros**: 100% waterproof; lightweight with super-lightweight options; easy to pack; good breathability; **Cons**: Printed pattern is prone to degrade over time; waterproof laminate is still partially exposed and can be contaminated with dirt and skin oils
3-Layer	Advanced waterproof membrane laminated between a range of face fabrics and lightweight backing fabrics	**Pros**: Top end material; most breathable; high durability; great protection; lightweight backing fabric improves comfort, moisture absorbency and abrasion resistance; stretch (mechanical and elastic) options available **Cons**: Expensive; heavier than most 2.5-layer materials
Soft shell	Woven blend of nylon and elastane	**Pros**: Extremely breathable; water-resistant; excellent range of motion, **Cons**: Water-resistant, not waterproof;

Content adapted from The Outdoor Gear Exchange Blog post "How to Choose Rainwear," n.d.

2.3.1 Porous Media

Porous media refers to materials that exhibit networks of randomly distributed pores and passageways (channels and capillaries) connecting the two sides of the material. Porous media is widely studied in various branches of applied sciences. Fluid flow through porous media is considered in filtration, acoustics, geomechanics, hydrogeology, biology and material science among other fields. The materials are permeable to air and water vapor in suitable

pressure gradients and are generally characterized by a solid fraction and void fraction (or porosity). Most fabric materials have a solid volume fraction less than 0.5, leaving ample voids for heat and moisture transmission (Obendorf, 2010).

Laminated microporous membrane fabrics, offer the same windproof and waterproofness of traditional solid and coated fabrics used for outdoor apparel, yet demonstrate improved moisture vapor transport (R. Lomax, 2009). First introduced by Gore-Tex, the most commonly used microporous membranes today are made by mechanically expanding polytetrafluoroethylene membranes (known as ePTFE membranes). The performance of multi-layered laminates is largely dependent on the endlessly variable pore structure (max, min, mean pore size, % pore volume, pore shape, pore distribution, tortuosity), physical properties (thickness) and transport properties (air permeability, water vapor permeability) of the membrane.

Physical Characteristics of Gore-Tex: Generally, for a microporous membrane to withstand liquid penetration, the pores should be no larger than 1μm and to maximize the water vapor transmission the porosity should be as high as possible (G. R. Lomax, 2007). A typical 30 micron ePTFE membrane has a 20:80 solid to void fraction ratio (R. Lomax, 2009) and has about 'nine billion pores per square inch, with the largest pore being 0.2 microns' (Tanner, 1979).

2.3.2 Mass Transport in Microporous Membranes

The transport of molecules across membranes is a well-studied phenomenon since it is an essential process in many living organisms. Pore geometry inherently makes most membranes selectively permeable, as small

molecules easily pass through the tiny pores while larger molecule cannot fit through the pores and are blocked. Microporous membranes are incorporated into waterproof fabrics because it makes them breathable. The two essential mass transport properties governing breathability are gas permeability and diffusion.

Air permeability is used to quantify how easily air is able to penetrate a fibrous material. On a garment level, it represents a standard performance requirement, as wind can considerably decrease thermal comfort by increasing convective heat loss. When air penetrates a garment, there is a reduction in thermal insulation due to 1) an increase in circulation on the surface and under the clothing; 2) an increase in microclimate air renewal rate; 3) air passing through pores causes trapped air to no longer be stationary. Additionally, external air speed helps reduce the thickness of the microclimate and the boundary layer formed at the outer surface of the garment, further reducing the resistance to convective heat and mass transfer. Fabrics with low air permeability are therefore desired for outerwear applications, as they improve thermal insulation and protection. Air permeability also contributes to mass transport, as ventilation of the microclimate (replacing warm humid air with cooler dryer air) can increase the rate of moisture transfer.

The theory of air flow through porous materials is based on Darcy's law, which relates the velocity of a fluid flowing through a porous column is directly proportional to the pressure difference and inversely proportional to the length of the column (Grant & Groenevelt, 1993). Interestingly, larger pores contribute the most to air permeability, as the flow rate of air varies as the fourth power of the pore radius. Darcy's law can be summarized

$$Q = k\frac{A}{\mu h}p$$

where Q is the flow rate in volume at average pressure (cc/sec), k the permeability constant (Darcys), A the area of the sample, h the thickness of the sample(cm), μ the viscosity of the fluid (cP, 0.185 for air) and p the differential pressure across the sample.

In practice, fabric sample thickness is often surprisingly difficult to measure, and a common source of error. To reduce measurement error, the inverse of permeability, gas flow resistance, is often used in its place. Resistance can be calculated by dividing thickness h by the permeability constant k. Resistance measures are more intuitive, as gas flow resistance is positively correlated with thermal resistance for any given textile material.

Water vapor diffusion is measure of how easily fabric or clothing permits the transport of water vapor molecules. Diffusion is a passive process by which water vapor molecules migrate from one area to an area of lower ambient water vapor pressure. In clothing, it is usually driven by the pressure gradient that exists between the microclimate and the surrounding environment. Performance garments designed for active applications require construction materials with high water vapor permeability. If the diffusion rate is too slow, water vapor generated from evaporative cooling is unable to escape to the microclimate and condenses back into water, which leads to sensations of discomfort.

Diffusion is widely characterized using Fick's Law of Diffusion, which states the rate of transfer per unit area is proportional to the concentration gradient measured normal to the area:

$$J = D_{eff}\nabla C$$

where J is the diffusive flux, D_{eff} is the effective diffusivity and ∇C is the concentration gradient. In order to apply Fick's law, the effective diffusivity tensor must first be experimentally determined by one of a variety of test methods in commonly used (Jianhua Huang & Xiaoming Qian, 2008).

Similar to air permeability, water vapor diffusion is often reported as a resistance, in this case the intrinsic resistance to mass transfer by diffusion. Intrinsic resistance to water vapor diffusion can be calculated by dividing the thickness h by the effective diffusivity D_{eff}. With minimal reordering, Darcy's law can easily be used to calculate intrinsic resistance:

$$R_i = \frac{\Delta C}{J}$$

2.3.3 Directional Transport Properties

One does not have to look far to find living examples of directional transport properties. Scientists who study biomimicry, the study of and emulation of nature for sustainable innovation, have highlighted a number cell membranes found in living organisms exhibit directional transport properties (Xie, Chen, Marszalek, & Tsong, 1997). Evolved and optimized for survival in extreme environmental conditions over thousands of years, plant leaves offer fast water transport to cope with rapid transpiration. Plant leaves are comprised of diverse double-layered nano/micro porous structures across species, habitats and biodiversity (H. Kim, Kim, Huh, Hwang, & Lee, 2015). Inspired by water vapor transport in leaves, Kim et. al. designed a simple model for solute transport through of double layered porous hydrogel structures.

More recently, researchers have observed similar asymmetric transport phenomenon in synthetic structures. Matthias and Müller demonstrated both numerically and experimentally that pore geometry induced asymmetric transport properties based on Brownian motion in etched silicon membranes with ratcheted pore structure (Matthias & Muller, 2003).

Siwy et. al. demonstrated similar asymmetric diffusion currents, using a salt solution and a polymer membrane with a single conically shaped nanopore with a specific pore gradient, but was heavily dependent on surface charge (Siwy et al., 2005). It has also been shown that gradients of varying porosity and pore size across the thickness of layered materials can lead to preferential liquid transportation from one side to another (Bal, Fan, Sarkar, & Ye, 2011).

Shaw et. al. demonstrated that asymmetric diffusion across membranes could be induced simply based on pore geometry, as geometric and kinetic constraints were enough to hold "blocker" particles (Shaw, Packard, Shorter, & Swinney, 2007). Their results suggest that porous membranes with stratified porosity (or void fraction gradients), the geometry alone may be capable of causing diffusion asymmetries in the direction of higher porosity gradient with less geometric limitations (Shaw et al., 2007).

Finally, Valdés-Parada and Alvarez-Ramirez developed a volume averaging approach to describe asymmetric diffusion in porous media (Valdés-Parada & Alvarez-Ramírez, 2011). Through simple geometries simulating a channel with increasing magnitude, they showed that asymmetric diffusion was strongly dependent on the geometries of the pore gradients.

2.3.4 Improving Moisture Management in Microporous Membranes

Based on the above transport phenomena, there may be room to improve membrane performance by increasing material porosity, reducing fiber diameter, aligning in-plane fiber orientation or altering the pore structure. The goal of this research is two fold; first, to experimentally explore how these parameters affect transport properties in single layer nanofiber membranes, and second, to investigate and maximize asymmetric directional transport properties in multilayered textile materials for applications in breathable fabrics, protective fabrics and filtration/separation materials.

2.4 Electrospun Membranes

One possible solution to increase thermal comfort of protective clothing may be the incorporation of electrospun membranes into laminate fabrics. Electrospinning is a process capable of spinning various polymers and nanoparticles into nanofibers with diameters in the range of 10-1500nm. When run continuously, the technique can produce super thin membrane-like nanowebs with extremely small pore sizes. Experimentally electrospun nanowebs have been shown to have excellent structural properties (Ahn, H.W. et al., 2011) and have demonstrated low air permeability and high moisture permeability, offering minimal impedance to moisture vapor diffusion and comparing favorably with transport properties of conventional waterproof-breathable fabrics (Gibson, Schreuder-Gibson, & Rivin, 2001b).

Electrospun Nanofibers: Electrospinning is a novel fiber spinning method capable of producing continuous nanofibers from polymer solutions. When a high voltage capable of overcoming surface tension forces is applied to a

suspended polymer solution droplet, a fine jet of liquid shoots out toward a grounded collector. As it travels across a set collection distance, the polymer jet is stretched into a fiber that is drawn out due to the whipping action and the solvent evaporates drying the fiber. When it reaches the collector, the continuous fibers assemble into an interconnected web of fibers. These mats form membrane like structures with high surface area to weight ratios, high porosity and incredibly small pore sizes.

Morphology: There are several important spin parameters that impact nanofiber morphology. While many spin parameters may be polymer specific, Chowdhury and Stylios specifically examined the experimental effect of different parameters on Nylon 6 fibers (Chowdhury & Stylios, 2010). Increases in polymer solution concentration (wt.%) and solution flow rate (ml/hr) were found to have a direct affect on fiber diameter. Fiber diameter was affected inversely by increases in electric potential (kV) and collection distance (cm). They found optimal spin parameters to produce uniform nanofibers with an average diameter of 924 nm to be 20 wt.% solution concentration, 15kV applied voltage, 0.20 ml/hr and a collector distance of 8 cm.

Transport Properties of Electrospun Nanofibers: Gibson et al extensively studied the transport properties of electrospun membranes and found the convective gas flow resistance to be quite high when compared with traditional clothing fabrics, largely due to the small fiber/pore size (Gibson et al., 2001b). The high air resistance did not obstruct the water vapor diffusion required for evaporative cooling. In fact, electrospun membranes were found to present minimal impedance to moisture transport, performing significantly better than

commercially available membrane laminates currently used in protective clothing. The research also found the membranes to exhibit good tensile strength.

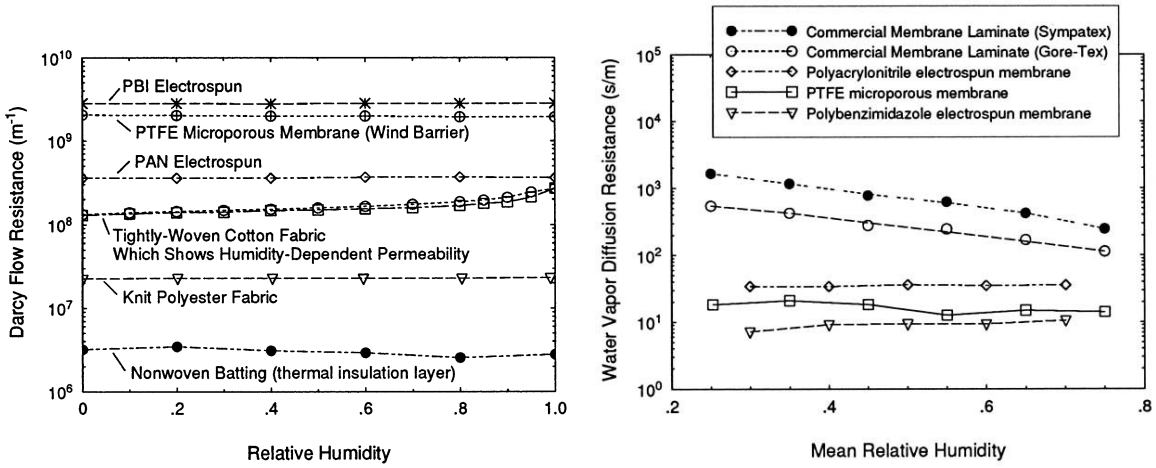

Figure 2.3 Electrospun membranes demonstrate high gas flow resistance and excellent water vapor diffusion resistance when compared to traditional waterproof breathable materials (Gibson et al., 2001b).

2.4.1 Advantages of Electrospun Membranes in Performance Clothing

Lee and Obendorf analyzed pore size distributions to determine the feasibility of using electrospun nanofiber membranes in protective clothing applications (S. Lee & Obendorf, 2007b). Their research found electrospun membranes performed in the range of traditional nonwoven fabrics and microporous membranes. Additionally, they found thin layers of electrospun polyurethane significantly improved barrier protection performance against challenge liquids. Their findings suggest engineered electrospun materials with specialized pore sizes could be used to improve specialized protection needs and thermal comfort in protective clothing.

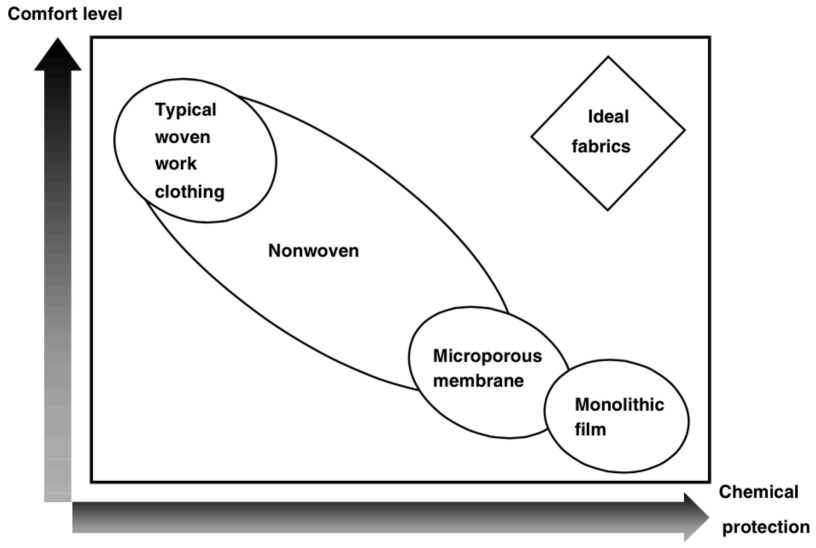

Figure 2.4 "Window of opportunity" as identified by Lee and Obendorf (S. Lee & Obendorf, 2007a).

Ahn, Park and Chung also examined the waterproof and breathable properties of commercially available nanowebs applied to outdoor clothing (Ahn, H.W. et al., 2011). They found the water vapor transmission of garments constructed with nanoweb membranes to perform better than those made with traditional PTFE membranes. Water penetration results were acceptable for rain protection, however they did not test as well as conventional PTFE membranes.

Previous research indicates that the use of electrospun membranes in protective clothing may be useful to construct materials with barrier and transport properties previously unobtainable. Gibson et al found that "electrospun layers present minimal impedance to moisture vapor diffusion required for evaporative cooling" (Gibson et al., 2001b).

Another potentially significant manufacturing benefit to using electrospun nanofibers for protective clothing is that they can be sprayed directly onto a 3D form. Many protective garments suffer from seam-sealing issues. One possible

solution to this longstanding construction issue may be the direct application of an electrospun membrane on the inside of a garment, eliminating the need for seam tape all together.

2.4.2 Modeling Transport in Electrospun Nanofiber Membranes

The subject of heat and mass transfer through fibrous materials is well studied (Farnworth, 1986; Hosseini & Tafreshi, 2010). Classic models for gas permeability however, were developed for orderly packed coarse fibers and generally rely on the assumption of continuous flow around the fiber and no-slip at the fiber surface (Grafe & Graham, 2003). When fiber diameters are on the same scale as the mean free path of the gas molecules however (65nm for air in standard temperature and pressure), gas velocity at the surface of the fiber can no longer be assumed to be zero. Traditional transport models therefore underestimate gas transport of electrospun nanofiber membranes since they inadequately account for slip flow at the fibers surface and random fiber distribution.

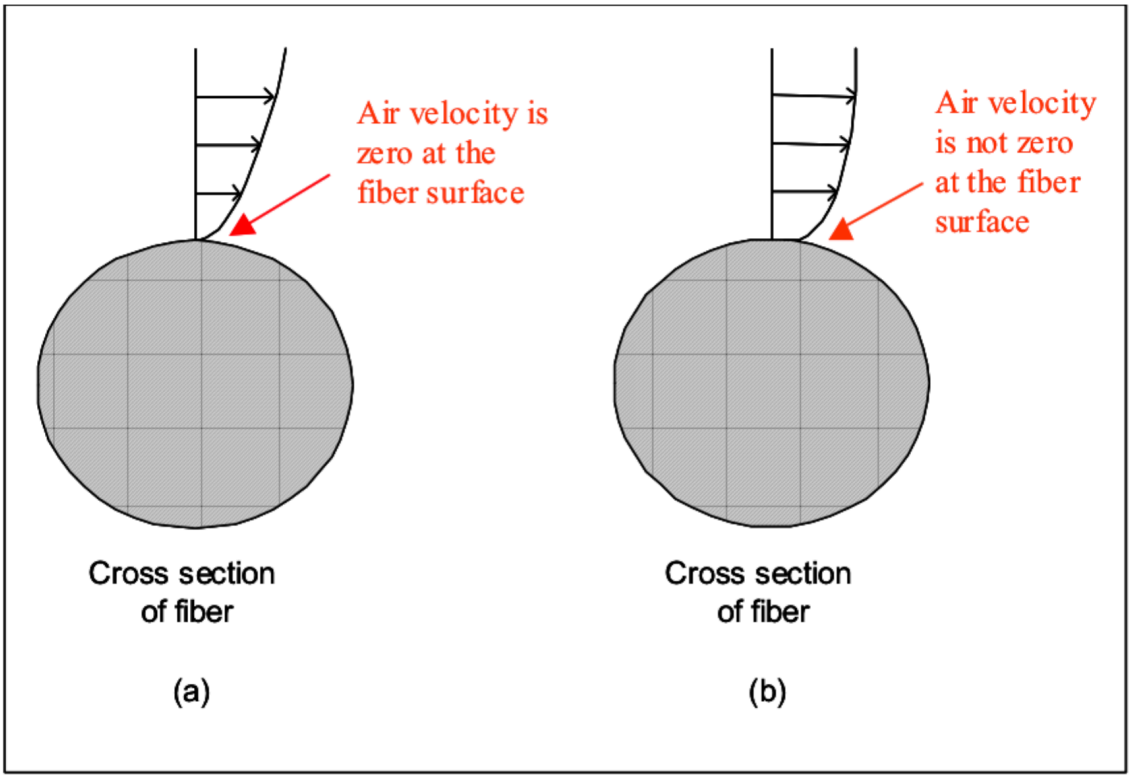

Figure 2.5 Velocity profiles at the fiber surface for (a) assuming non-slip flow; and (b) accounting for slip flow. Figure adapted from *Polymeric Nanofibers in Air Filtration Applications* (Grafe & Graham, 2003).

To extend the useful range of continuous flow theory, models may account for the effects of slip flow by incorporating the Knudsen number (Kn). The Knudsen number is a ratio of the gas mean free path to fiber radius that describes the importance of air molecule movement near the fiber surface to the overall flow field.

$$Kn = \frac{\lambda}{r}$$

Shou et. al. developed a model for through-plane permeability of randomly distributed electrospun nanofiber that considered slip-flow (Shou et al., 2014). Considering orthogonal fibers in place of parallel ones and using a single factor to quantify the effect of random fiber distribution on flow behavior, the model

only requires two easily measured geometrical factors: fiber radius and fiber volume fraction. Shou's model illustrates the expected increase in gas permeability caused by slip effect and randomly distributed fibers.

As with gas flow resistance, water vapor resistance is a combination of fabric layers and air layers that has been well studied over the past 50 years. Existing theoretical models describing the effective diffusivity are equally limited however, focusing largely on 1D with regular fiber arrays. Nonwoven nanofibers are inherently randomly distributed, often in a 2 or 3-dimensional plane, thus traditional models tend to over-estimate the effective diffusivity. Shou et. al. proposed a new model that extended existing 1D models for regular fiber alignments to 1D random fiber alignments, then used the local diffusivities to determine 2D and 3D diffusivities based on water vapor mixing laws (Shou et al., 2013). Shou's models for 1D, 2D and 3D randomly located fibers are given by:

$$\text{1D:} \quad \frac{D_{eff}}{D_b} = \frac{\varepsilon}{2.7-1.7\varepsilon}$$

$$\text{2D:} \quad \frac{D_{eff}}{D_b} = \frac{\varepsilon}{6}\left(\frac{3.7-1.7\varepsilon}{2.7-1.7\varepsilon} + \frac{4}{3.7-1.7\varepsilon}\right)$$

$$\text{3D:} \quad \frac{D_{eff}}{D_b} = \frac{\varepsilon}{6}\left(\frac{4.7-1.7\varepsilon}{2.7-1.7\varepsilon} + \frac{9}{6.4-3.4\varepsilon}\right)$$

2.4.3 Improving Transport Properties Through Nanofiber Alignment

Fiber alignments of electrospun nanofiber mats are naturally random. Membranes with randomly aligned fibers have a mixture of large and small pore sizes and generally exhibit higher air permeability, as gas transport is dictated by the largest pore size. Mechanical devices can be used however to obtain ordered structures, such as the use of a rotating drum collector to create aligned fibers.

Carnell et al incorporated an auxiliary counter electrode to create an electric field around a rotating collection drum (Carnell et al., 2008). Matthews et al experimented with the effect of rotation speed on electrospun collagen fiber alignment. For rotation speeds were below 500 rpm, the resulting fiber alignment remained random. When the rotation speed was increased to 4500 rpm however, the fibers began to align along the axis of rotation (Matthews, Wnek, Simpson, & Bowlin, 2002). Additional research has explored the mechanical properties of aligned nanofibers (K. W. Kim, Lee, Khil, Ho, & Kim, 2004). Interestingly, very little attention has been given to the effect of in-plane fiber alignment on transport properties to date.

3 Materials and Methodology

Two different experiments were performed in order to address the effect of in-plane alignment on 1) air and water vapor transport properties and 2) directional transport properties in multilayered materials with positive and negative pore size gradients.

In the first experiment, six unique nylon 6 membranes were produced at two different weight percentages (15wt% and 20wt%) and three different alignments (collected at 100, 1000 and 2500 RPM). Fiber characterization was performed and the resulting transport properties were analyzed.

A second experiment was conducted to explore the directional transport properties in multilayered membranes. At first, three multilayered nylon nanofiber membranes (15wt% spun over 20wt%) collected at 100, 1000 and 2500 RPM were produced. Successful initial results led to additional testing; in which three randomly oriented poly(vinylidene fluoride-*co*-tetrafluoroethylene) (PVDF-TFE) membranes were spun and layered over a polypropylene (PP) microfiber, polyethylene-nylon (PET-nylon) composite microfiber, and nylon woven fabric. Similar characterization tests were performed and transport properties were measured in both directions to assess asymmetric behavior.

3.1 Materials

Nylon-6 pellets ((C6H11NO)n) and 88-91% formic acid (CH2O2) were obtained from Sigma-Aldrich (St. Louis, MO) in addition to acetone (C3H6) from Mallinckrodt Chemicals (Phillipsburg, NJ) for electrospinning. 20-mL BD luer-lok plastic syringes were purchased from First Choice Medical Supply (Richland, MS) along with 23-gauge blunt tip dispensing needles from CML Supply

(Lexington, KY). White silicone tubing was ordered from amazon.com for the programmable syringe pump.

Magnetic stir bars, 20-mL glass vials, and Parafilm were all purchased at the Cornell Chemical Supply Room (Ithaca, NY) and used to mix polymer solutions for electrospinning on a heated stirring hot plate.

Uncoated ripstop nylon fabric (1.9oz, 70 Denier), used as a substrate while electrospinning, was ordered from Seattle Fabrics (Seattle, WA) and cut into 9-inch by 5¾-inch swatches using a soldering iron to prevent fraying.

3.2 Methodology

3.2.1 Electrospinning

All electrospinning processes in this experiment were conducted in a custom-built electrospinning apparatus. The spinning setup allowed users to control the electric potential (both positive for the syringe tip and negative for the collection drum), syringe pump flow rate, and collection drum rotational speed in a closed space, to limit potential error and improve repeatability. The high voltage power supply used for the syringe tip was capable of producing 0 to +25kV while the negative high voltage supply attached to the collection drum was capable of producing 0 to -3kV. The programmable syringe pump had 0.1mL/hr accuracy for flow rates between 0 and 1 mL/hr.

Rotating Collection Drum: A custom built rotating drum collector was devised to collect aligned nanofibers. An electric step motor controlled by an external supply allowed for variable collection speeds from 100 to 6000 RPM. Initial pilot studies showed greatest degree of alignment at 2500 RPM, thus

membranes were collected at 100, 1000, and 2500 RPM for alignments labeled "slow", "mid", and "fast".

Electrospinning Solution Preparation: Formic acid and acetone were combined to create a 7:3 mixture. Nylon-6 pellets were added to the solution and dissolved in both 15 wt.% and 20 wt.% concentrations. Magnetic stir bars were then used to help mix the solutions while they were heated over a hot plate for 20 minutes. After 20 minutes of heating, the heating element was shut off, and the solutions were mixed for a period of no less than 24 hours. All solutions were used for electrospinning within 5 days of preparation.

Dimethylformamide (DMF) and acetone were combined to create a 7:3 mixture. An 8:2 mixture of PVDF and TFE was then dissolved in the solvent create a 14wt% solution that was heated on a stirring hot plate for 3 hours at 65˚c.

Membrane Production: Single layer membranes were produced using both 15wt.% and 20wt.% solution concentrations at three different collection speeds: slow (100rpm), mid (1000 rpm) and fast (2500rpm). A positively charged syringe tip (23 gauge, 17kV) was placed 10cm away from the negatively charged (-1kV) rotating drum collector. The syringe pump was set to 0.3mL/hr and left for a period of 8 hrs. A total of 6 single layer membranes were produced.

Multilayer membranes were also created, spinning the two different polymer concentrations directly on top of one another, at the same three speeds as the single layer membranes. Membranes 7,8,9 represent the multilayered membranes. Direction 1 will be used to denote the negative pore gradient direction (20wt% then 15wt%) and direction 2 will be used to denote the positive pore gradient (15wt% then 20wt%).

PVDF-TFE: Three unique single layer membrane were produced using the prepare solution. Spin parameters were +14kV, -3kV potential, 16cm spin distance, 0.4mL/hr flow rate. Membranes were spun onto aluminum foil at a collection speed of 16 RPM for a period of 23hrs.

3.2.2 Membrane Characterization

Thickness: Membrane thickness was measured using a Brown & Sharpe 599-100 Digital Caliper, range 0.004 mm and accuracy 0.004mm (Stockholm, Sweden). Membranes of 1, 2, 4, 8, and 16 layers were repeatedly measured 6 times at various locations then an average was taken. Values of thickness are reported in mm.

Mass: Due to the lightweight nature of the electrospun membranes, three 5 X 5 cm samples were massed from each material. All three samples were massed on a digital lab scale (0.0001g accuracy) and an average value was determined.

Density: Sample density was calculated my multiplying mean mass measurements by sample volume (5cm X 5cm X thickness).

Porosity: Total porosity is the fraction of the bulk material volume that is not occupied by solid materials. When the solid volume is unknown or cannot be measured, it is possible determine porosity by measuring the sample density and comparing it to the density of the solid polymer material:

$$\phi = 1 - \frac{\boldsymbol{\rho_{media}}}{\boldsymbol{\rho_{polymer}}}$$

Not included in the measurement of porosity are key physical properties of the pore structure, such as pore size, geometry, distribution and connectivity.

Scanning Electron Microscopy: Scanning electron microscopy (SEM) images were taken using a ZEISS 1550VP Field Emission SEM (Oberkochen, Germany). Small 5mm by 5mm samples were adhered to aluminum studs using double-faced carbon tape then prepared for imaging with carbon sputter coating. Three images at randomly selected locations within each sample were captured at 5K, 15K, 50K and 100K magnification.

Fiber Diameter: Fiber diameter was determined using the 15K magnification SEM images and ImageJ software (National Institutes of Health). Diameters of 50 randomly selected fibers per image were recorded, resulting in 150 unique measurements per membrane.

Fiber Orientation: Fiber orientation was measured using orientationJ, a plugin for the ImageJ software (National Institutes of Health). OrientationJ evaluates every pixel within the SEM image based on structure tensors. Orientation histograms are then built using select pixels that are greater than a user defined minimum coherency (70%) and have at least 10% of normalized energy. These histograms accurately represent the distribution of individual fiber alignments (-90 to 90 degrees). The weighted standard deviation of the alignment distribution from the mean (axis of rotation) was then used to quantify fiber orientation.

3.2.3 Transport Properties

Data Analysis: All transport property data was analyzed using the open source R language and in the RStudio software environment. Both the R language and RStudio are freely available under the GNU General Public License.

Water Vapor Permeability: Upright and inverted cup tests are easy methods to calculate water vapor permeability (WVP). Nylon nanofiber membranes were tested using upright cup tests before it was determined inverted cup tests yielded more accurate results. Upright cup tests offer limited accuracy because an air gap exists between the surface of the water within the cup and the test sample. Though using a measured amount of water helps maintain equal air gap thicknesses, it is impossible to ensure equal resistances across cups. This is certainly a downside, as the resistance of air is often several times greater than the resistance of the test sample.

For the PVDF-TFE nanofiber membranes and PP microfiber nonwovens, mass flux *J* was determined employing the inverted cup test method using a Gore-Tex laminate ePTFE membrane to keep the material samples dry.

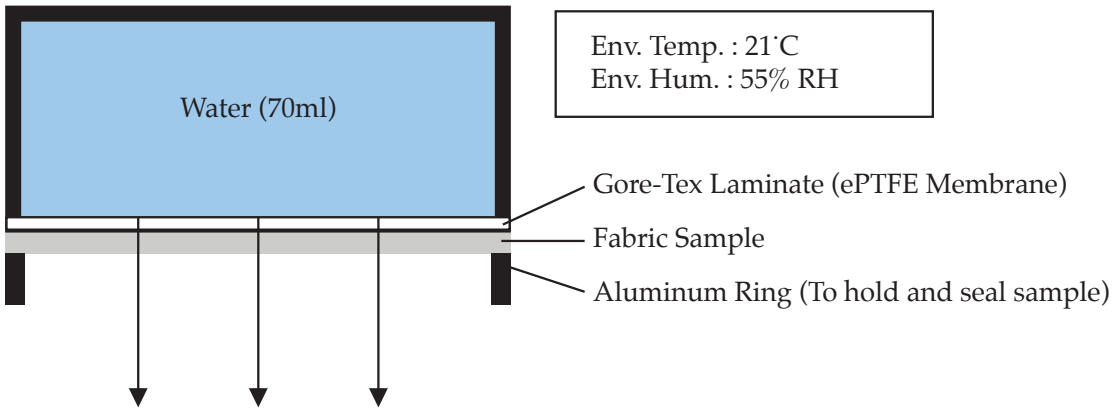

Figure 3.1 Principal of the inverted cup test for water vapor permeability testing.

Small dishes were filled with 70ml of distilled water. Gore-Tex laminate ePTFE membranes were glued to the top of the dish and allowed to dry overnight. Samples were then placed on top of the membranes and held in place

by protective rings. The rings were then secured in place using electrical tape. Dishes were massed then inverted and placed on a rotating tray in a climate-controlled room (73.0F, 55%). Dish assemblies were then conditioned for at least 3 hours, and subsequently massed every hour for a period of 4-6 hours. The mass loss was then used to determine the WVP or mass flux (J) using the following equation:

$$WVP = \frac{g \times 24}{t \times A} = mass\ flux = J = (\dot{m}/A)$$

where g = mass loss, t = elapsed time and A = sample area. Mass flux was in turn used to calculate the intrinsic resistance of the test material (R_i):

$$(R_i + R_{ePTFE}) = \left[\frac{\Delta \bar{C}}{(\dot{m}/A)}\right]$$

where R_{ePTFE} is the resistance of the membrane, $\Delta \bar{C}$ the water vapor concentration difference between the inside of the cup (RH=100%) and the climate controlled room (RH=55%).

Diffusion rates were measured for 0, 1, 2, and 3 layers of samples and averaged to calculate the mean resistance of the ePTFE membrane, which was subsequently subtracted from the 1, 2, and 3 layer values to determine the intrinsic resistance of a single layer of sample material. Directional materials were tested multiple times in both directions (micro over nano, nano over micro).

Air Permeability: Air permeability was collected using an 1100-AEHXL capillary flow porometer (Porous Media Inc., Ithaca, NY). Gas permeability test were conducted by increasing the pressure in a small chamber above the sample, while continuous measurements of the resulting flow through and pressure drop

across the dry sample were recorded. Flow rate (Q) and pressure drop (p_b-p_a) were then used to calculate Darcy's Permeability Constant (k) using the equation:

$$Q = -kA\frac{(p_b - p_a)}{(\mu h)}$$

where A is equal to the sample area, μ equal to the viscosity of air (0.0185cP) and h equal to the sample thickness. All calculations of Darcy's Permeability were conducted using R. The code used can be found in Appendix A.

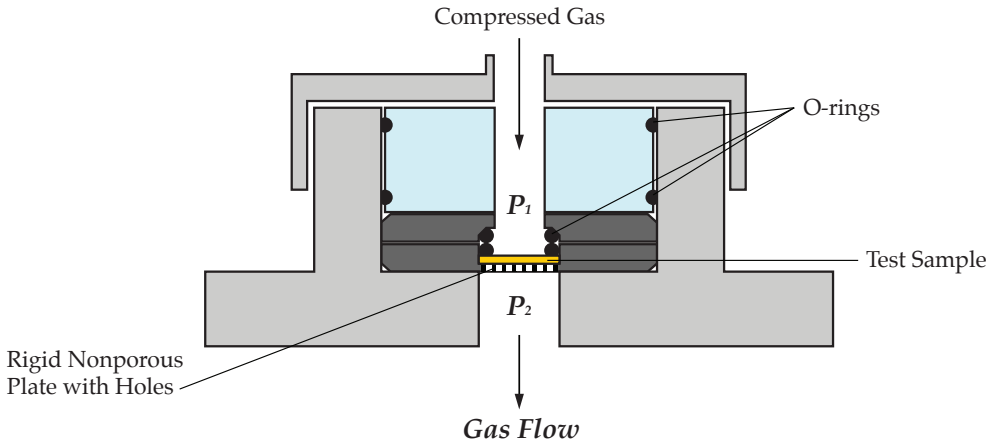

Figure 3.2 An illustrative look inside the sample chamber of a capillary flow porometer. Compressed gas of a known pressure is applied above (P1) and measured below (P2) along with the resulting gas flow (in cc/sec).

Capillary Flow Porometer: Pore size and pore size distribution data was collected using an 1100-AEHXL capillary flow porometer (Porous Media Inc., Ithaca, NY). Selwick oil with a known surface tension of 20.1 dynes/cm (Porous Media Inc., Ithaca, NY) was used to fully saturate 3 cm diameter circular samples of electrospun membranes. Multi layered membranes were tested in both directions (15-20, 20-15). A wet up/dry up test procedure was performed using PMI software to collect wet and dry curve data. From these two curves, PMI

software was used to calculate pore size and distribution using the following equation:

$$D = \frac{4\gamma cos\theta}{p}$$

where D is the pore diameter; γ the wetting agent surface tension (20.1); θ the contact angle of the wetting liquid; p the differential pressure.

4 Results and Discussion

4.1 Nylon Nanofiber Membranes

The first set of experiments was designed to test the effect of in-plane nanofiber alignment on air permeability and water vapor diffusivity. For each membrane sample, SEM images were used to quantify fiber diameter and fiber orientation (reported as the weighted standard deviation in degrees separating 150 randomly selected fiber angles from the axis of rotation). Thickness measurements and mass measurements were used to calculate density and porosity. Upright cup tests and the porometer data was used to calculate WVP and Air Permeability.

4.1.1 Nylon Nanofiber Characterization

Mean fiber diameters for membrane spun with 15 wt.% solution were 147.605 ± 38.808 nm while membranes made with 20 wt.% solution were found

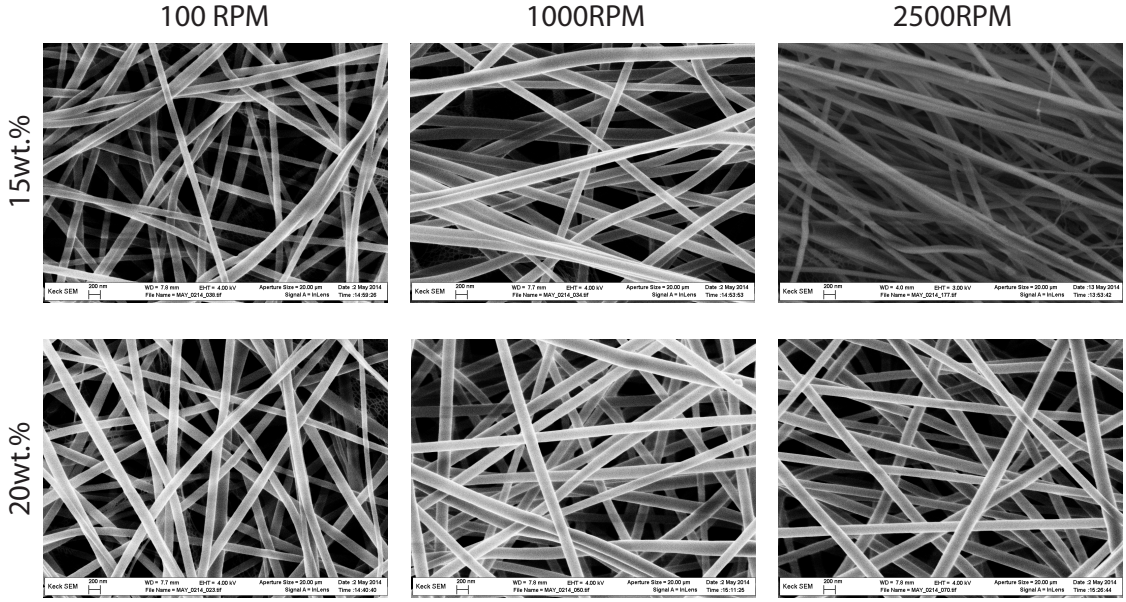

Figure 4.1 SEM image key at 50K magnification for nylon nanofiber membranes.

to have mean fiber diameters of 193.988 ± 36.317 nm. Because the thin nature of the electrospun membranes, thickness measurements, though seemingly simple, may have been problematic and represent a potential source of error when incorporated into air permeability and WVP measurements. Though all membranes were spun under similar conditions, thickness measurements between membranes varied roughly 30% in the 15wt.% membranes and greater than 50% for the 20wt.% membranes. Thickness measurements may be one source of error causing discrepancy in porosity measurements.

Table 4.1 Single layer nylon nanofiber membrane alignment study material summary: characterization and transport data

Sample	Mean Diameter (mm)	Thickness (mm)	Fiber Alignment	Density ϱ (g/cm^2)	Porosity φ	Mean WVP (g/m2/day)	Mean Air Permeability (Darcys)
Nylon wt15 slow	0.00016538	0.03113	47.08198	0.13919	0.87683	280.2639*	0.00421
Nylon wt15 mid	0.00019311	0.02412	41.69660	0.26261	0.76760	323.8605*	0.00424
Nylon wt15 fast	0.00012849	0.03405	30.41364	0.15663	0.86139	310.3663*	0.00411
Nylon w20 slow	0.00014894	0.03707	51.20430	0.16637	0.85277	339.4308*	0.00990
Nylon w20 mid	0.00019408	0.04287	41.99897	0.13802	0.87785	350.8489*	0.01002
Nylon w20 fast	0.00019477	0.01985	32.81093	0.19312	0.82910	309.3283*	0.00886

*WVP affected by air gap resistance present in upright cup test

4.1.2 Effect of Fiber Diameter on Single Layer Transport Properties

Membranes with larger fiber diameters were found to have higher air permeability, while the effect of fiber diameter on water vapor permeability was less noticeable. These findings are in line with existing models provided by Shou that describe transport properties in nanofiber materials. Models for air permeability are dependent on both porosity and fiber diameter, whereas models describing water vapor diffusion are only dependent on porosity.

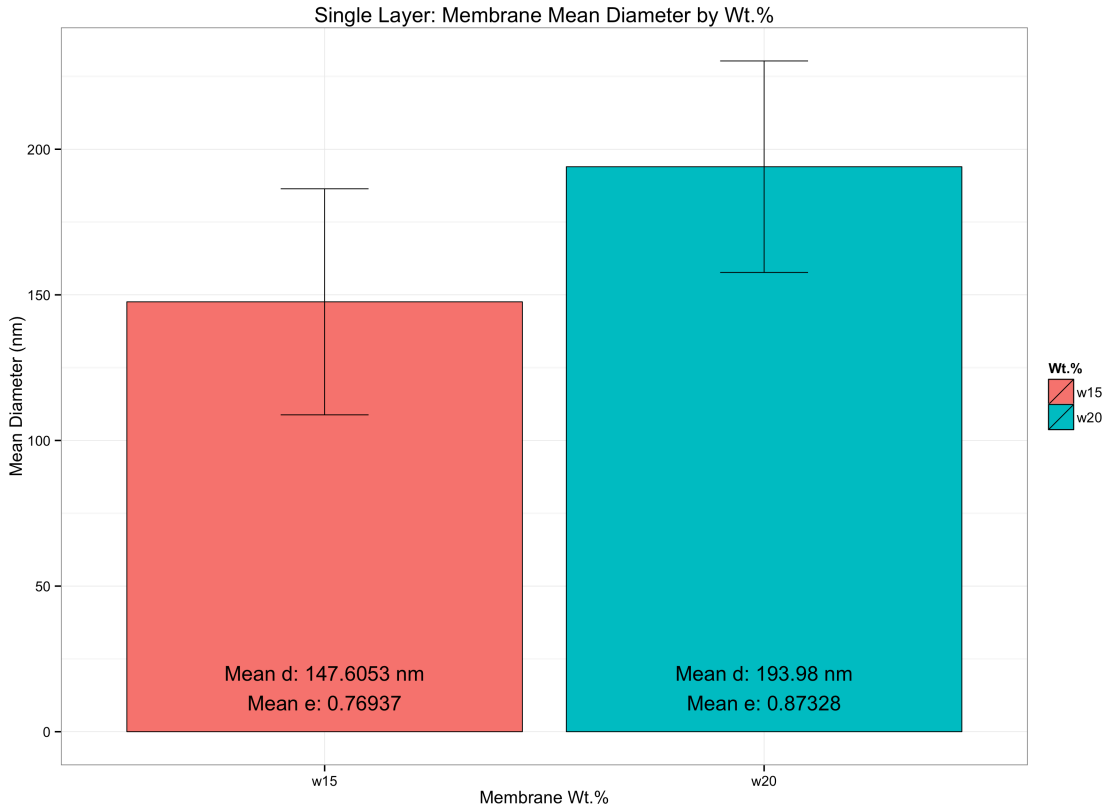

Figure 4.2 Effect of polymer solution concentration on nanofiber diameter (d) and porosity (e).

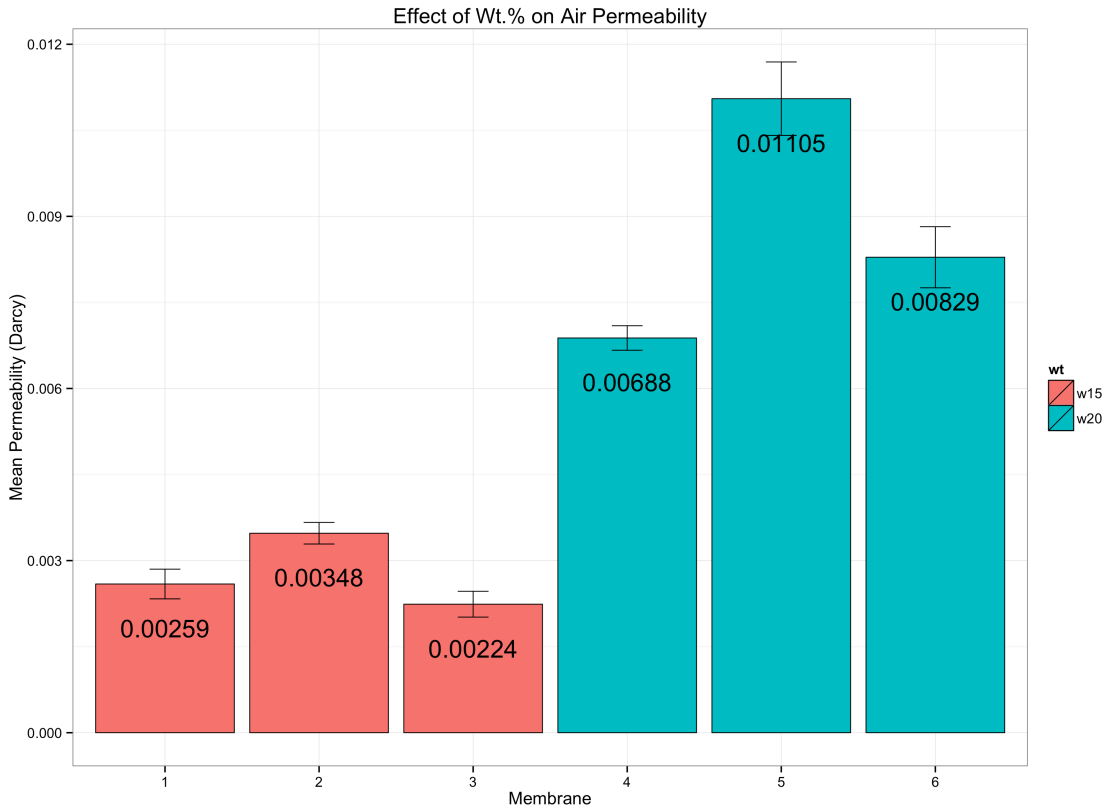

Figure 4.3 Effect of wt.% on air permeability of single layer nylon membranes.

It is worth noting that the water vapor permeability data in this experiment was measured using the upright cup test. One significant drawback of the upright cup test is that it does not account for the resistance of the air gap that exists between the surface of the water in the cup and the membrane. The water vapor permeability values presented above represent the combination of the membrane permeability and the boundary resistance between the surface of the water and the air gap. Diffusion rates are different for each membrane; therefore one cannot be certain that the air gap remains constant between cups. Additionally, the resistance between the surface of the water in the cup and the air within the cup is significantly greater than the resistance of the nanofiber

membrane. For these reasons, the water vapor permeability data presented here should only be used to compare samples in this test to one another.

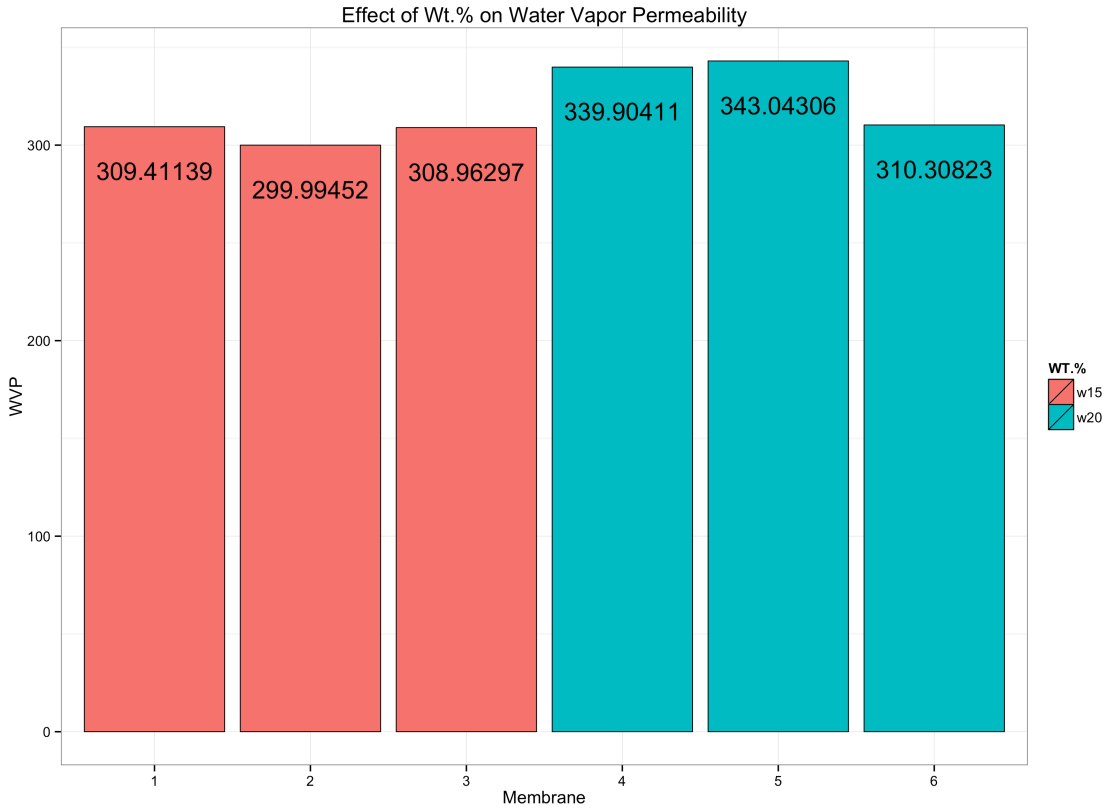

Figure 4.4 Effect of wt.% on water vapor permeability of single layer nylon membranes.

4.1.3 Quantifying Fiber Alignment

Fiber alignment, as measured in 150 randomly selected fibers in each SEM image, was quantified based on a weighted standard deviation of alignment distribution away from the axis of rotation. Membranes ranged from ~50 for slow collection speeds (random fiber distribution) to ~30 for fast collection speeds (improved fiber alignment). Membranes where then divided into groups according to collection speed and their transport properties were analyzed.

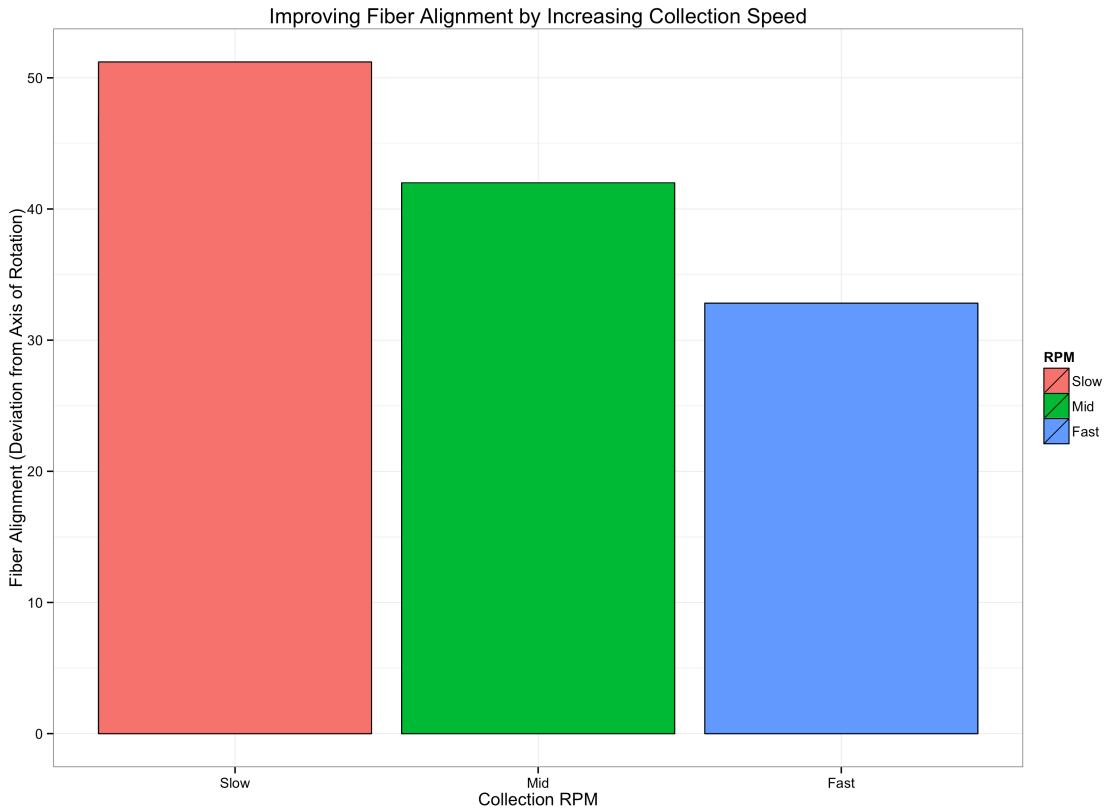

Figure 4.5 Fiber alignment, quantified as the weighted standard deviation of individual fiber orientation away from the axis of rotation, improving with increasing collection speeds.

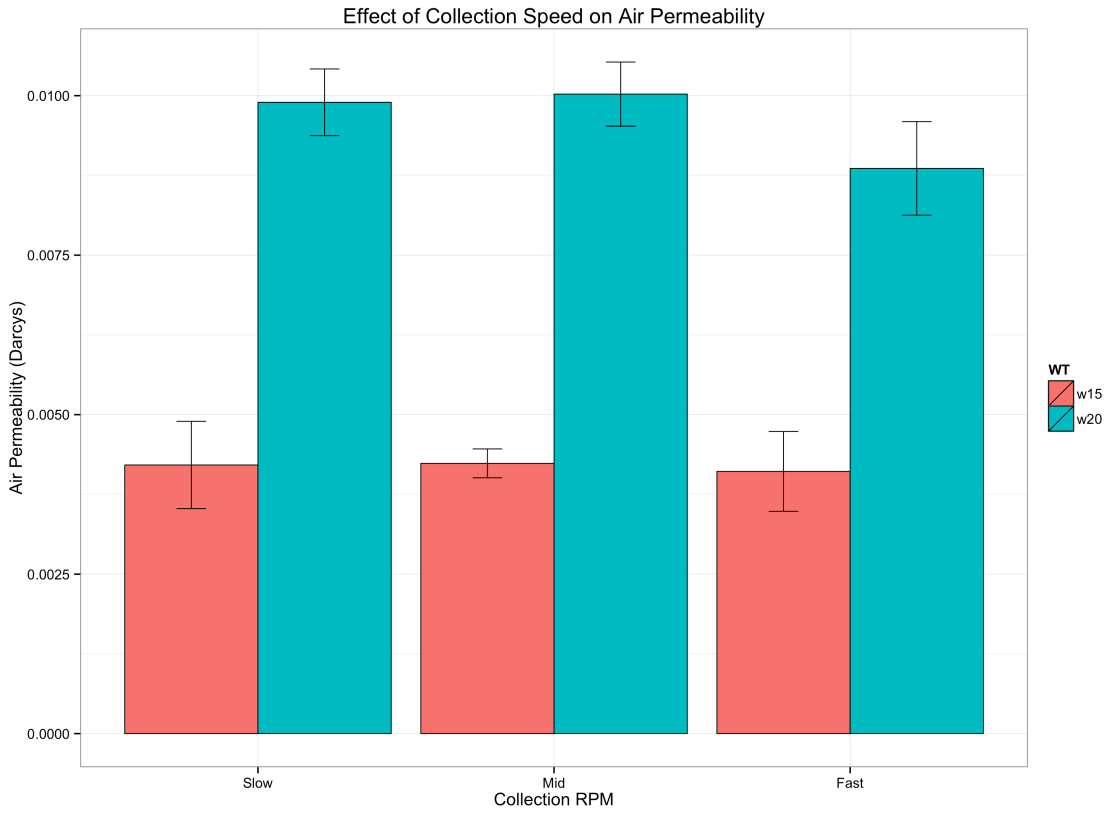

Figure 4.6 Effect of solution concentration and collector rotational speed on air permeability.

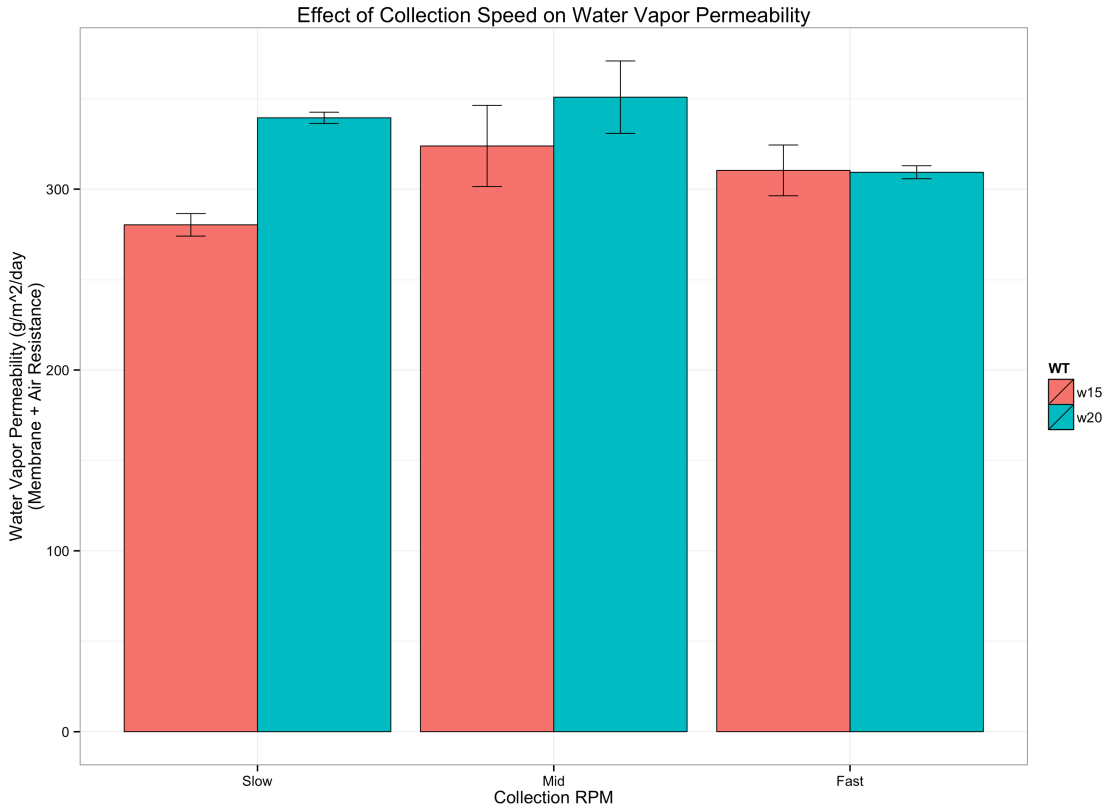

Figure 4.7 Water vapor permeability results were found unrelated to in-plane fiber alignment.

4.1.4 Effect of Fiber Alignment on Transport Properties

Results found in this study (experiment 1) suggest that there is no significant correlation between in-plane fiber orientation and air permeability or water vapor permeability. While these findings do not support the original hypothesis of this thesis, they are no less original and informative.

4.1.5 Directional Transport Properties of Multilayered Nylon Nanofiber Membranes

Multilayered membranes (15wt.% spun directly on top of 20wt.% membranes) were found to exhibit slight directional transport property preference in the direction of positive pore size gradient. The directional

difference fell within the measurement error, diluting the significance of the findings. It was theorized that this was due to the two pore sizes (15wt% and 20wt.%) were on the same magnitude (nano-nano), and that to better demonstrate the effect, materials of different magnitudes (nano-micro) would be required. The fact that the trend was repeatable across all repetitions and collection speeds however was deemed significant interest. It was upon these findings that a second experiment was designed with more practical materials for which pore sizes differed in magnitude.

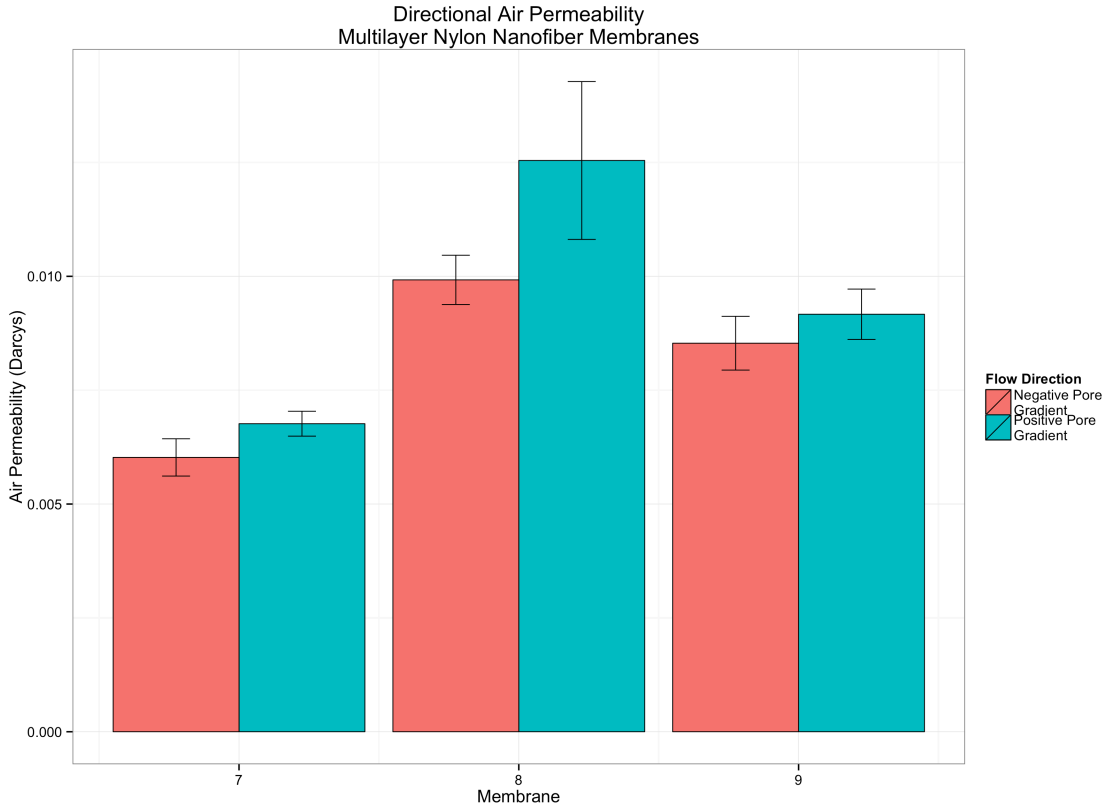

Figure 4.8 Multilayered nylon electrospun membranes with positive pore gradients (created by spinning 20wt.% solution directly over 15wt.% solution) found to exhibit slightly higher air permeability values.

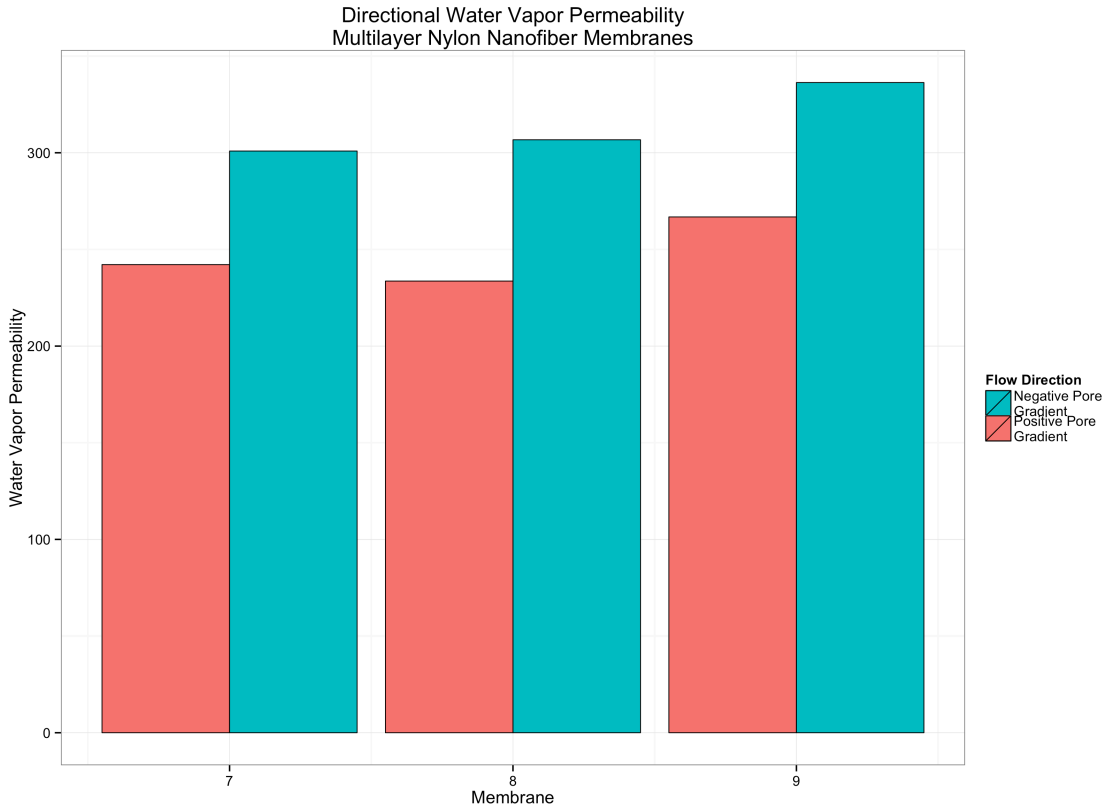

Figure 4.9 Directional water vapor permeability observed in the multilayered nylon electrospun membranes.

4.2 Directional Transport Properties

To further build on the unique findings of the multilayered nylon electrospun membranes, a second experiment was designed and conducted to further explore the directional transport properties. In an effort to exaggerate the effect, nanofiber membranes were layered with microfiber nonwovens, such that the difference in fiber diameter and individual transport properties would be an order of magnitude. Nano and Micro materials were combined in both increasing (positive) and decreasing (negative) pore size gradients directions.

4.2.1 Fiber Characterization

Two primary fibrous materials were selected for use in this experiment, a PP microfiber nonwoven material (mean fiber diameter 0.02347mm) and the electrospun PVDF-TFE membrane (mean fiber diameter 0.000522mm). Additional materials, a PET-Nylon composite nonwoven and a woven nylon fabric were also used in multilayered constructions to try and maximize the asymmetric effect.

Table 4.2 Single Layer Material Summary Characterization and Transport Data

Sample	Mean Diameter (mm)	Thickness (mm)	Density ϱ	Porosity φ	Mean WVP (g/m2/day)	Mean Air Permeability (Darcys)
PVDF Nanofiber	0.00052178	0.03783	0.35925	0.80042	10.72079	0.02293
PP Microfiber	0.02347400	0.07566	0.20420	0.78414	36.53938	6.94102
PET-Nylon Composite	0.06112000	0.23840	0.43122	NA	102.0609	4.960119
Nylon Woven	0.04972320	0.08910	0.69722	0.39372	NA	0.49844

4.2.2 Single Layer Transport Properties

Air permeability tests of single layers of each material were conducted on 10 unique samples. The results helped determine which samples were more structurally stable during the testing process. Large permeability variation seen in the composite and micro nonwovens suggests that either their thickness is not uniform or that the samples are deforming during testing. Results from the 10 unique air permeability tests are illustrated in Figure 4.10.

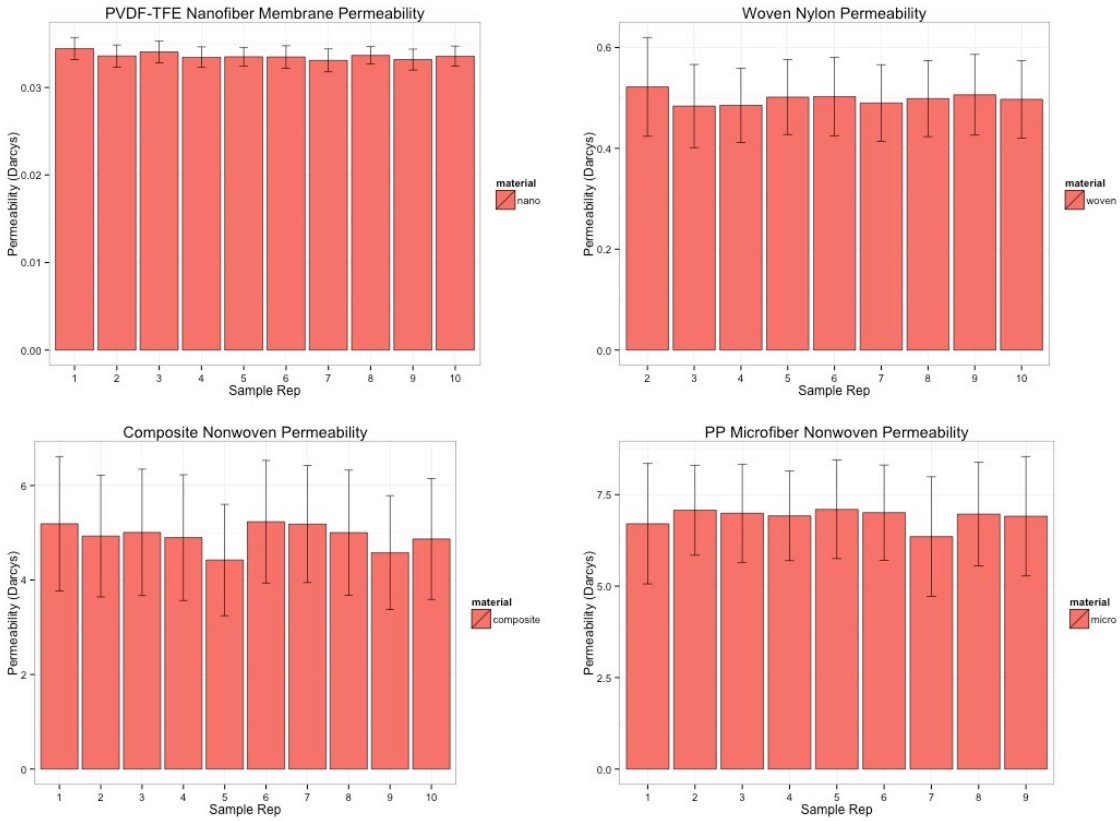

Figure 4.10 Single layer air permeability for PVDF-TFE nanofiber membranes, woven rip stop nylon fabrics, PET-Nylon composite nonwoven and PP microfiber nonwoven.

Inverted cup tests were also performed on the PP microfiber and the PVDF-TFE nanofiber to determine their intrinsic resistance (total resistance – PTFE membrane resistance). Intrinsic resistance of a single layer of microfiber nonwoven was found to be 36.53938 s/m while the nanofiber membranes were determined to be 10.72079 s/m. Resistance results are comparable with similar materials tested in previous research (Gibson et al., 2001b). Slight variation was unavoidable during these tests as the relative humidity in the testing lab was unable to stabilize.

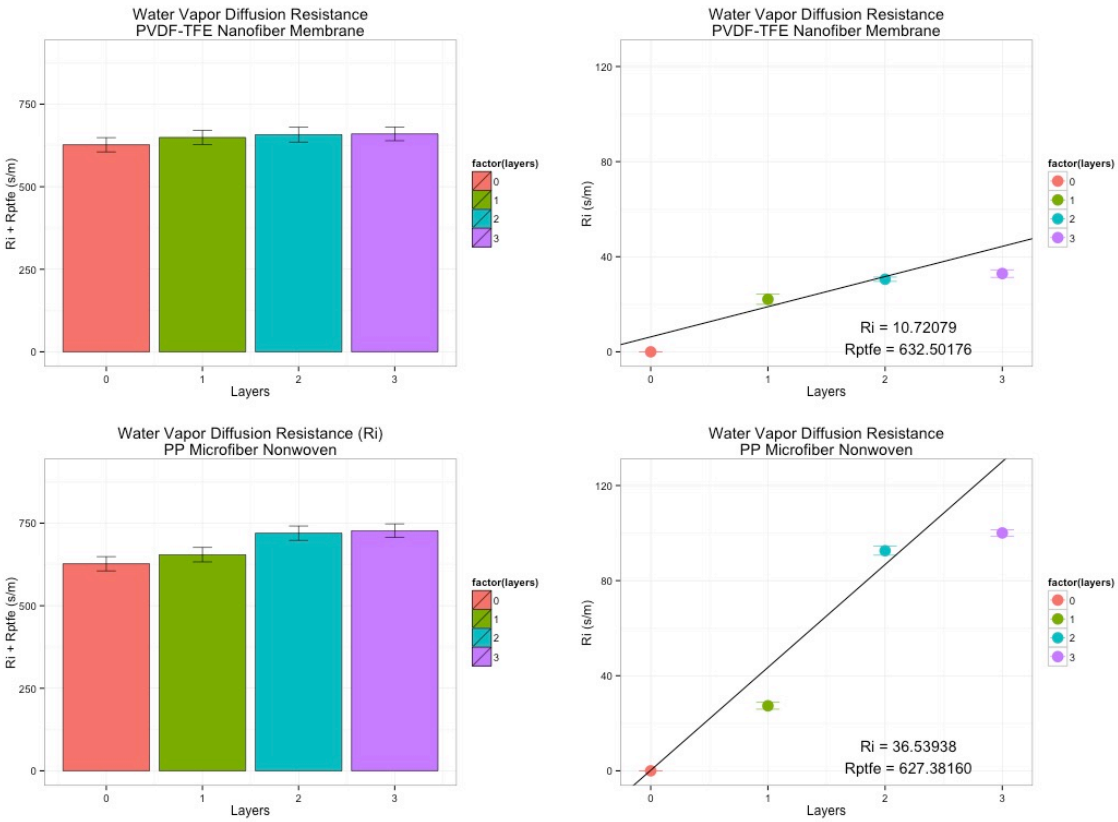

Figure 4.11 Water vapor resistance of PVDF-TFE nanofiber membranes (10.72 s/m) and PP Microfiber membranes (36.54 s/m).

4.2.3 Fitting Transport Data to Verify Models

Transport data for single layers of PVDF-TFE nanofiber membranes and PP microporous nonwovens were plotted against existing models. The experimental data was found to fit both diffusion and gas permeability models exceedingly well. The data fitting exercise was both useful to help add validity to the models and ensure the single layer data was accurate and within the sensible range.

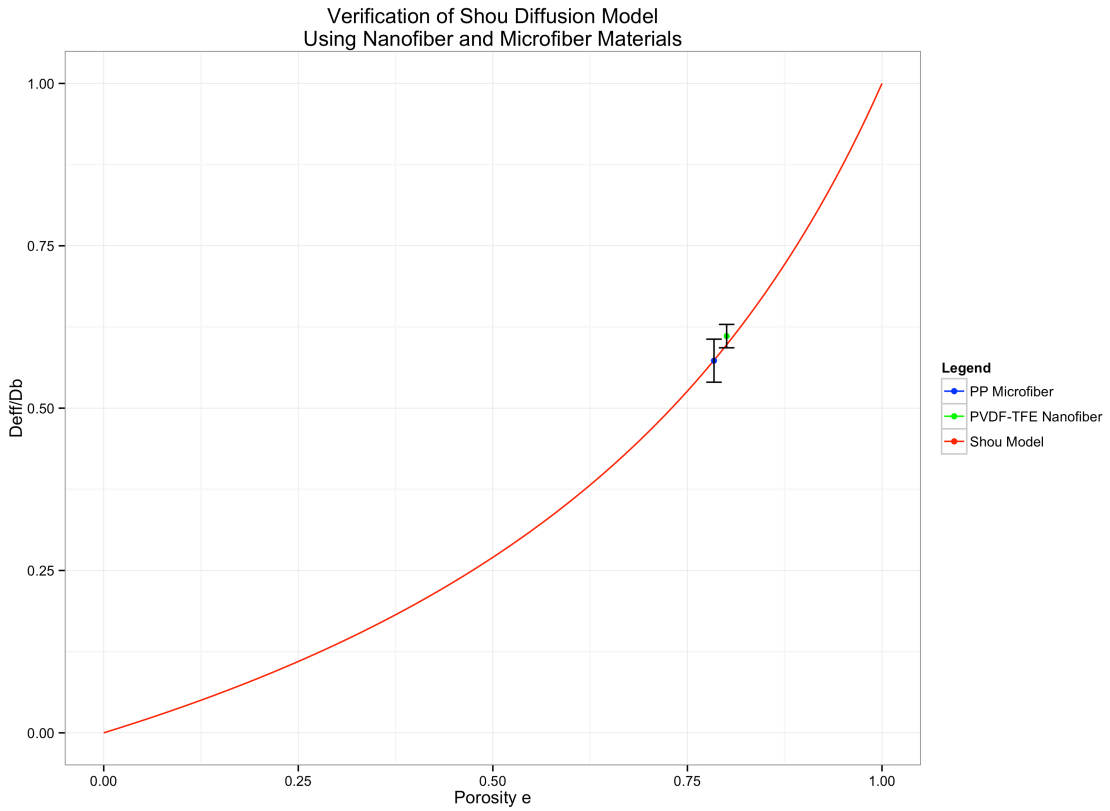

Figure 4.12 Verification of Shou diffusion model using electrospun membranes and microfiber nonwoven materials.

Four different flow regimes exist around fibers, depending on their diameter. The Knudsen number for the PVDF-TFE nanofiber material was determined to be 0.499, placing it in the transition regime. Materials with fiber diameters in the transition regime will likely experience the effect of slip-flow, and it must therefore be considered when modeling gas permeability.

Table 4.3 There are four different regimes of flow around a fiber.

Flow Regime	Knudsen Range
Continuum Flow Regime	< 10^-3
Slip-flow Regime	10^-3 – 0.25
Transition regime	0.25 – 10
Free molecule regime	> 10

Adapted from (Hosseini & Tafreshi, 2010)

The PVDF-TFE nanofiber material was found to have a Knudsen number of 0.440 (65nm/147.615nm). This value places the material in the lower range of the transition flow regime. In this range, slip flow is quite likely occurring. Comparing the transport data for the nanofiber membrane, Shou's permeability model was found to accurately predicted the air permeability.

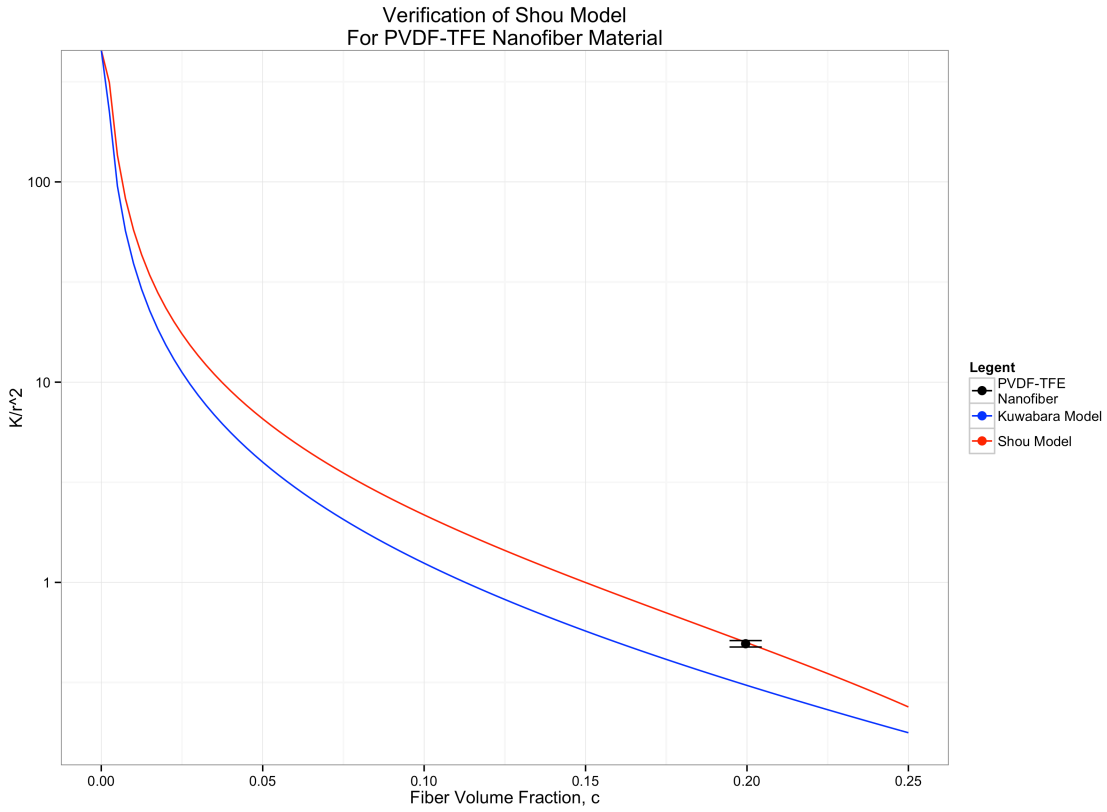

Figure 4.13 Verification of Shou permeability model using PVDF-TFE electrospun membrane.

4.2.4 Directional Air Permeability

Although permeability is generally assumed to be directionally uniform across porous materials, repeatable, directional air permeability measurements were observed in six different fabric combinations (composite-nanofiber,

microfiber-nanofiber, woven-nanofiber, composite-2nanofibers, microfiber-2nanofibers, and woven-2nanofibers). An asymmetric ratio (permeability in positive pore gradient direction / air permeability in negative pore gradient direction) was used to determine the maximum asymmetric effect. Interestingly, the composite nonwoven single layer tests were found to have the least structural stability. It was theorized that perhaps this lack of stability lead to the material collapsing, causing a decrease in porosity and air permeability.

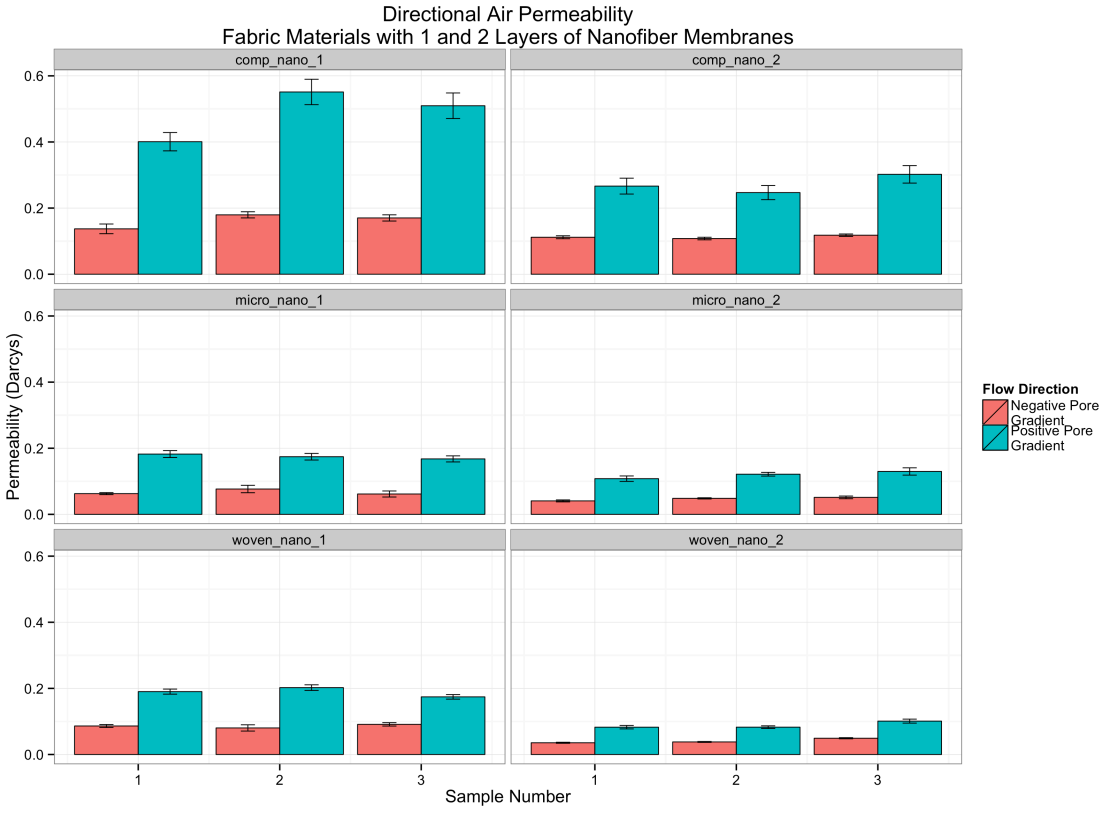

Figure 4.14. Directional air permeability of multilayered constructions. The greatest directional asymmetry was observed layering the PVDF-TFE nanofiber membrane over a highly permeable composite nonwoven material.

4.2.5 Directional Diffusion

Asymmetric diffusion has been observed in multilayered fibrous materials. It is theorized that the transport mechanisms may be similar to those found in nature, most familiarly in biological cell membranes. Asymmetric diffusion has also been

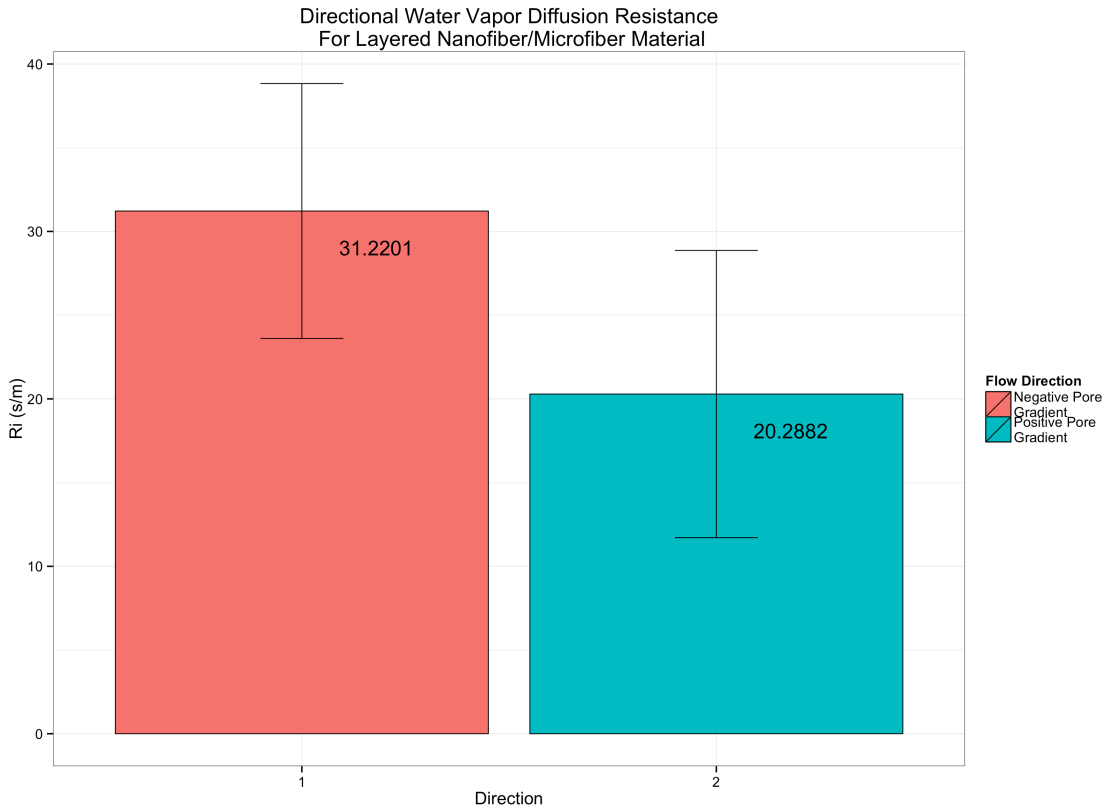

Figure 4.15 Directional water vapor diffusion resistance (s/m) for the PVDF-TFE nanofiber/PP microfiber multilayered construction.

4.2.6 Asymmetric Ratio

An asymmetric ratio was calculated to quantify the directionality of the materials. Larger asymmetric ratio values represent greater differences in directional flow.

Table 4.4 Asymmetric ratio of directional flow.

Sample	Material	Asymmetric Ratio
1	composite - nano	3.000912
2	micro - nano	2.610378
3	micro - 2 nano	2.555772
4	composite - 2 nanc	2.414324
5	woven - nano	2.198827
6	woven - 2 nano	2.170749

4.2.7 Directional Transport Property Theory Discussion

The exact mechanisms causing the directional preference are still largely unexplained. While directional diffusing has previously been documented in natural materials (and a few synthetic materials), most previous research has been focused on the transport of ions or larger particles than water vapor molecules (~0.4nm). Two hypothetical mechanisms will be presented here based on our findings.

Relative Velocity Theory: It is known from fluid dynamics that for any object, drag forces act opposite to direction of relative motion. For an object moving in air, this force is sometimes called air resistance. Unlike frictional resistive forces, air resistance is proportional to velocity in smooth, laminar flows and the proportional to the squared velocity in chaotic, turbulent flows. Drag forces decrease fluid velocity relative to the solid object in the fluid's path.

When a fluid passes through a constriction, basic conservation of mechanical energy laws deem it will experience an increase in velocity and a decrease in static pressure. In the case of multilayered nanofiber/microfiber materials when exposed to equal flow rates, one would expect the fluid velocity

in the nanofiber to be greater (smaller pore size, greater constriction) than the microfiber pores. Applying the concept of air resistance, increased air velocity should result in increased apparent gas permeability resistance. Data from the single layer membranes and microfiber nonwoven was evaluated to confirm this assumption:

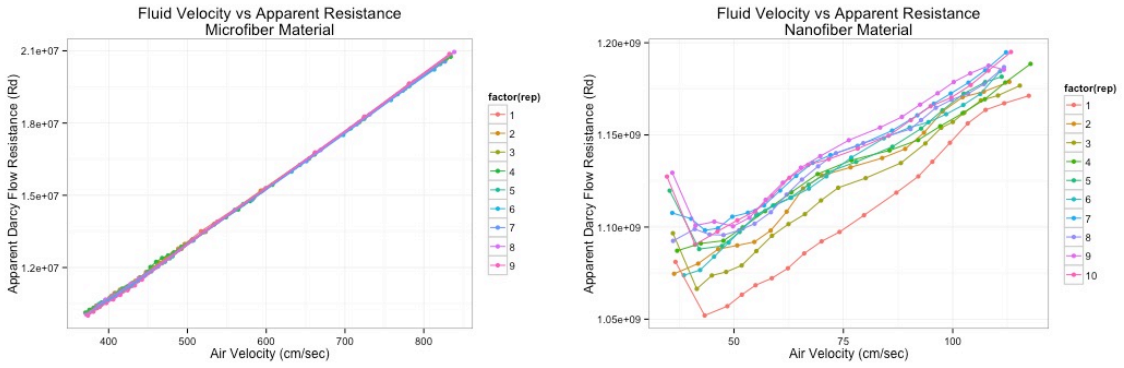

Figure 4.16 Air velocity vs apparent resistance for microfiber and nanofiber membranes for small pressure drops. Both appear to be linear.

A simple linear regression of apparent resistance ~ velocity for both the microfiber and nanofiber materials was run to yield the effect of velocity on the resistance of each material. The model suggests that for an increased airflow velocity of 1 cm/s, the microfiber resistance experienced a 1.70% while the nanofiber resistance increase 0.12%. To apply both these findings and the fluid dynamic theory to multilayered membranes, we must consider the mean fluid velocity as it first interacts with each surface. Direction 1 will be considered first.

As illustrated below, airflow first encounters the microfiber membrane with an initial velocity of V_1. Resistance at this interface (*M1*) as the air interacts with the fiber surface is assumed to be a function of this initial relative velocity, V_1. As the airflow is constricted into the microfiber pores, the flow velocity

increases to V_2. Next, this slightly increase flow velocity encounters the nanofiber material resulting in a second resistance (*M2*), a function of the new slightly faster V_2. The total resistance for Direction 1 is thus the sum, *M1+M2*.

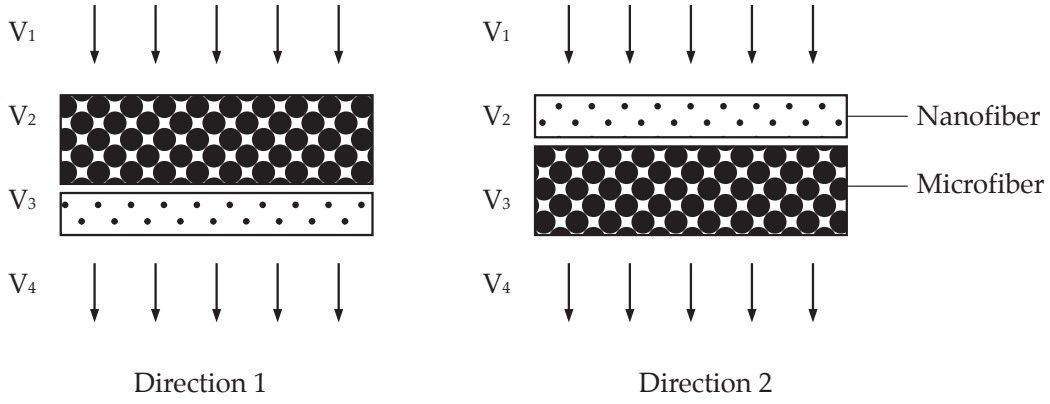

Figure 4.17 Asymmetric transport illustration of transport property testing directions.

When Direction 2 is considered, the airflow of initial velocity V_1 first encounters the nanofiber membrane and is met with an initial resistance (*N1*). This flow is more severely constricted as it enters the tiny pores of the nanofiber membrane, increasing the overall velocity V_2. When V_2 exits the nanofiber material and interacts with the microfiber, the increased velocity results in a new resistance (*N2*) that is nearly 2% per cm/s greater than the microfiber resistance experienced in Direction 1.

Flow Stability Theory: Our second theory looks at the type of flow entering the second (or bottom) layer of the multilayered constructions. As hinted at previously, air resistance is proportional to velocity in laminar flows and the proportional to velocity squared in turbulent flows. Perhaps, the flow entering the bottom nanofiber layer in Direction 1 is turbulent, having first been

broken up by the large microfibers. This would make the resistance in layer 2 proportional to the velocity squared. In Direction 2 however, the small pore sizes and the slip flow past the nanofiber yield a slower, more laminar flow, resulting in the resistance of layer 2 being proportional to the velocity.

Material Stability Theory: As the single layer test results illustrated, the error bars associated with the air permeability tests can be interpreted as a measure of the materials stability. While the nanofiber demonstrated repeatable results, the microfiber experienced a significant amount of variation. It is entirely possible that part of the directional differences in air permeability was due to the materials deforming. In Direction 1 when the microfiber was unprotected by the relatively air impermeable nanofiber membrane, the microfiber may have simply be compressed, reducing the porosity and increasing it's overall resistance. Similarly, in Direction 2, the pores of the nanofiber may have actually enlarged when unprotected by the microfiber membrane, thus increasing it's air permeability.

5 Conclusions / Future Work

5.1 Transport Properties of Aligned Nanofibers

Electrospun nylon 6 membranes were successfully produced at three different and measurable levels of fiber alignment. Air permeability and water vapor diffusion test results suggest there is no apparent relationship between in-plane fiber alignment and breathability. If this idea is to be further tested, higher levels of alignment must be achieved. To that end, the addition of a auxiliary electrode may be implemented in the electrospinning setup to achieve improved fiber alignment.

5.2 Model Verification

The models for gas permeability and water vapor diffusion in nanofiber materials presented by Shou et. al. were found to accurately predict our experimental data. The verification was limited however, as relatively few porosities were considered. To strengthen future verifications, a wider range of nanofiber porosities is recommended. To this end, different polymers could be spun or samples could be pressed, packing the fibers closer together and reducing pore volume.

5.3 Asymmetric Transport

Multilayered nylon nanofiber/nanofiber membranes with varying porosity and air permeability were found to exhibit mild asymmetric transport properties. Further verification of these findings should be considered, spinning more layers nanofibers representing a greater range of diameters and porosities. This may be accomplished by altering spin parameters, using different polymer

solutions, or considering bi-component spinning with a degradable element (such as PEO) that may be removed after spinning.

Multilayered nanofiber/microfiber membranes were found to exhibit varying degrees of asymmetric transport properties. The directionally dependent transport effect was found to be more apparent for materials with larger pore size differences. Additional water vapor transport data should be collected in a more stable climate to confirm observations. While the effect was repeatable for both air permeability and water vapor diffusion, the explanatory theory deservers further attention. Each of the three proposed theories deserves careful analysis and consideration. In order to fully explain the asymmetric effective, more data must be collected and the effective range of the asymmetric ratio must be increased, as effected by porosity, fiber diameter, thickness and pore size gradient. Additional data should also make the development of a model possible, to describe the observed asymmetric phenomena.

Ahn, H.W., Park, C.H., & Chung, S.E. (2011). Waterproof and breathable properties of nanoweb applied clothing. *Textile Research Journal*, *81*(14), 1438–1447. http://doi.org/10.1177/0040517510392462

Bal, K., Fan, J., Sarkar, M. K., & Ye, L. (2011). Differential spontaneous capillary flow through heterogeneous porous media. *International Journal of Heat and Mass Transfer*, *54*(13–14), 3096–3099. http://doi.org/10.1016/j.ijheatmasstransfer.2011.02.048

Carnell, L. S., Siochi, E. J., Holloway, N. M., Stephens, R. M., Rhim, C., Niklason, L. E., & Clark, R. L. (2008). Aligned Mats from Electrospun Single Fibers. *Macromolecules*, *41*(14), 5345–5349. http://doi.org/10.1021/ma8000143

Chowdhury, M., & Stylios, G. (2010). Effect of experimental parameters on the morphology of electrospun Nylon 6 fibres. *International Journal of Basic & Applied Sciences*, *10*(06), 116–131.

Das, B., Das, A., Kothari, V. K., Fanguiero, R., & De Araújo, M. (2008). Effect of fibre diameter and cross-sectional shape on moisture transmission through fabrics. *Fibers and Polymers*, *9*(2), 225–231.

Farnworth, B. (1986). A numerical model of the combined diffusion of heat and water vapor through clothing. *Textile Research Journal*, *56*(11), 653–665.

Ghaddar, N., Ghali, K., & Williams, J. T. (2009). Designing for ventilation in cold weather apparel. *Textiles for Cold Weather Apparel*, 131–151.

Ghali, K., Ghaddar, N., & Jones, B. (2006). 11 - Phase change in fabrics. In N. Pan & P. Gibson (Eds.), *Thermal and Moisture Transport in Fibrous Materials* (pp. 402–423). Woodhead Publishing. Retrieved from http://www.sciencedirect.com/science/article/pii/B9781845690571500119

Gibson, P., Schreuder-Gibson, H., & Rivin, D. (2001a). Transport properties of porous membranes based on electrospun nanofibers. *Colloids and Surfaces A: Physicochemical and Engineering Aspects*, *187*, 469–481.

Gibson, P., Schreuder-Gibson, H., & Rivin, D. (2001b). Transport properties of porous membranes based on electrospun nanofibers. *Colloids and Surfaces A: Physicochemical and Engineering Aspects*, *187–188*(0), 469–481. http://doi.org/10.1016/S0927-7757(01)00616-1

Grafe, T. H., & Graham, K. M. (2003). Nanofiber webs from electrospinning. In *Nonwovens in Filtration-Fifth International Conference, Stuttgart, Germany* (pp. 1–5). Retrieved from http://www.thefutureisnear.org/student_research/current_research/documents/filtration/052026(Filtration).pdf

Grant, C. D., & Groenevelt, P. H. (1993). Air permeability. *Soil Sampling andMethods of Analysis, Martin Carter (ed.), Lewis Publishers*. Retrieved from http://www.hse.niordc.ir/uploads/86_106_Binder5.pdf

Haghi, A. K. (Ed.). (2011). *Heat and mass transfer in textiles*. [Montreal]: WSEAS Press.

Havenith, G. (1999). Heat balance when wearing protective clothing. *Annals of Occupational Hygiene*, *43*(5), 289–296.

Holmér, I. (2005). Textiles for protection against cold. In *Textiles for Protection* (pp. 378–397). Camebridge: Woodhead Publishing.

Holmer, I. (2011). 16 - Cold weather clothing and comfort. In G. Song (Ed.), *Improving Comfort in Clothing* (pp. 412–426). Woodhead Publishing. Retrieved from

http://www.sciencedirect.com/science/article/pii/B9781845695392500168

Hosseini, S. A., & Tafreshi, H. V. (2010). Modeling permeability of 3-D nanofiber media in slip flow regime. *Chemical Engineering Science*, *65*(6), 2249–2254. http://doi.org/10.1016/j.ces.2009.12.002

How to Choose Rainwear. (n.d.). Retrieved from http://gearx.com/blog/knowledge/technical-outerwear-apparel/how-to-choose-rainwear/

ISO 7730. (1994). ISO 7730: Ergonomics of the thermal environment. International Organization for Standardization. Retrieved from http://aliquantum.rs/wp-content/uploads/2011/11/ISO-7730-1994.pdf

Jianhua Huang, & Xiaoming Qian. (2008). Comparison of Test Methods for Measuring Water Vapor Permeability of Fabrics. *Textile Research Journal*, *78*(4), 342–352. http://doi.org/10.1177/0040517508090494

Kessler, M. (2012, April). Insane in the Membrane. *Outside Magazine*.

Kim, H., Kim, H. J., Huh, H. K., Hwang, H. J., & Lee, S. J. (2015). Structural design of a double-layered porous hydrogel for effective mass transport. *Biomicrofluidics*, *9*(2), 024104. http://doi.org/10.1063/1.4914383

Kim, K. W., Lee, K. H., Khil, M. S., Ho, Y. S., & Kim, H. Y. (2004). The effect of molecular weight and the linear velocity of drum surface on the properties of electrospun poly (ethylene terephthalate) nonwovens. *Fibers and Polymers*, *5*(2), 122–127.

Lee, S., & Obendorf, S. K. (2007a). Barrier effectiveness and thermal comfort of protective clothing materials. *Journal of the Textile Institute*, *98*(2), 87–98. http://doi.org/10.1533/joti.2005.0143

Lee, S., & Obendorf, S. K. (2007). Transport properties of layered fabric systems based on electrospun nanofibers. *Fibers and Polymers*, *8*(5), 501–506. http://doi.org/10.1007/BF02875872

Lee, S., & Obendorf, S. K. (2007b). Use of Electrospun Nanofiber Web for Protective Textile Materials as Barriers to Liquid Penetration. *Textile Research Journal*, *77*(9), 696–702. http://doi.org/10.1177/0040517507080284

Lomax, G. R. (2007). Breathable polyurethane membranes for textile and related industries. *Journal of Materials Chemistry*, *17*(27), 2775. http://doi.org/10.1039/b703447b

Lomax, R. (2009). 4 - Coating and laminating fabrics for cold weather apparel. In J. T. Williams (Ed.), *Textiles for Cold Weather Apparel* (pp. 56–83). Woodhead Publishing. Retrieved from http://www.sciencedirect.com/science/article/pii/B978184569411150004X

Mackowiak, P. A. (2000). Temperature regulation and the pathogenesis of fever. *Principles and Practice of Infectious Diseases*, *6*, 703–718.

Matthews, J. A., Wnek, G. E., Simpson, D. G., & Bowlin, G. L. (2002). Electrospinning of Collagen Nanofibers. *Biomacromolecules*, *3*(2), 232–238. http://doi.org/10.1021/bm015533u

Matthias, S., & Muller, F. (2003). Asymmetric pores in a silicon membrane acting as massively parallel brownian ratchets. *Nature*, *424*(6944), 53–57. http://doi.org/10.1038/nature01736

Morton, W. E., & Hearle, J. W. S. (2008). Physical Properties of Textile FIbres. In W. E. Morton & J. W. S. Hearle (Eds.), *Physical Properties of Textile Fibres* (pp. 1–81). Woodhead Publishing. Retrieved from

http://www.sciencedirect.com/science/article/pii/B9781845692209500019

Obendorf, S. K. (2010). Improving personal protection through novel materials. *AATCC Rev*, *10*, 44–50.

Onofrei, E., Rocha, A. M., & Catarino, A. (2011). The influence of knitted fabrics' structure on the thermal and moisture management properties. *Journal of Engineered Fibers and Fabrics*, *6*(4), 10–22.

Pan, N. (2008). 6 - Sweat management for military applications. In E. Wilusz (Ed.), *Military Textiles* (pp. 137–157). Woodhead Publishing. Retrieved from http://www.sciencedirect.com/science/article/pii/B9781845692063500067

Rengasamy, R. S. (2011). 8 - Improving moisture management in apparel. In G. Song (Ed.), *Improving Comfort in Clothing* (pp. 182–215). Woodhead Publishing. Retrieved from http://www.sciencedirect.com/science/article/pii/B9781845695392500089

Rossi, B. (2009). Comfort-and-thermoregulatory-requirements-in-cold-weather-clothing.

Scheurell, D. M., Spivak, S. M., & Hollies, N. R. S. (1985). Dynamic surface wetness of fabrics in relation to clothing comfort. *Textile Research Journal*, *55*(7), 394–399.

Shaw, R. S., Packard, N., Schröter, M., & Swinney, H. L. (2007). Geometry-induced asymmetric diffusion. *Proceedings of the National Academy of Sciences*, *104*(23), 9580–9584.

Shou, D., Fan, J., & Ding, F. (2013). Effective diffusivity of gas diffusion layer in proton exchange membrane fuel cells. *Journal of Power Sources*, *225*, 179–186. http://doi.org/10.1016/j.jpowsour.2012.10.039

Shou, D., Ye, L., & Fan, J. (2014). Gas transport properties of electrospun polymer nanofibers. *Polymer*, *55*(14), 3149–3155. http://doi.org/10.1016/j.polymer.2014.05.016

Siwy, Z., Kosińska, I., Fuliński, A., & Martin, C. (2005). Asymmetric Diffusion through Synthetic Nanopores. *Physical Review Letters*, *94*(4). http://doi.org/10.1103/PhysRevLett.94.048102

Song, G. (2009). Thermal insulation properties of textiles and clothing. *Textiles for Cold Weather Apparel*, 19.

Song, G. (Ed.). (2011). Copyright. In *Improving Comfort in Clothing* (p. iv). Woodhead Publishing. Retrieved from http://www.sciencedirect.com/science/article/pii/B9781845695392500193

Tanner, J. C. (1979). Breathability, Comfort and Gore-Tex Laminates. *Journal of Industrial Textiles*, *8*(4), 312–322. http://doi.org/10.1177/152808377900800408

Valdés-Parada, F. J., & Alvarez-Ramírez, J. (2011). A volume averaging approach for asymmetric diffusion in porous media. *The Journal of Chemical Physics*, *134*(20), 204709.

Weather Records. (2015, April 13). In *Wikipedia*. Retrieved from http://en.wikipedia.org/wiki/List_of_weather_records

Williams, J. T. (Ed.). (2009). Introduction. In *Textiles for Cold Weather Apparel* (pp. xxi–xxvi). Woodhead Publishing. Retrieved from

http://www.sciencedirect.com/science/article/pii/B9781845694111500221

Xie, T. D., Chen, Y., Marszalek, P., & Tsong, T. Y. (1997). Fluctuation-driven directional flow in biochemical cycle: further study of electric activation of Na,K pumps. *Biophysical Journal*, *72*(6), 2496–2502.

Yoon, B., & Lee, S. (2011). Designing waterproof breathable materials based on electrospun nanofibers and assessing the performance characteristics. *Fibers and Polymers*, *12*(1), 57–64. http://doi.org/10.1007/s12221-011-0057-9